

Symbol-Level Precoding Through the Lens of Zero Forcing and Vector Perturbation

Yatao Liu[†], Mingjie Shao[†], Wing-Kin Ma[†] and Qiang Li[‡]

[†]Department of Electronic Engineering, The Chinese University of Hong Kong,
Hong Kong SAR of China

[‡]School of Information and Communication Engineering,
University of Electronic Science and Technology of China, Chengdu, China

March 1, 2025

Abstract

Symbol-level precoding (SLP) has recently emerged as a new paradigm for physical-layer transmit precoding in multiuser multi-input-multi-output (MIMO) channels. It exploits the underlying symbol constellation structure, which the conventional paradigm of linear precoding does not, to enhance symbol-level performance such as symbol error probability (SEP). It allows the precoder to take a more general form than linear precoding. This paper aims to better understand the relationships between SLP and linear precoding, subsequent design implications, and further connections beyond the existing SLP scope. Our study is built on a basic signal observation, namely, that SLP can be equivalently represented by a zero-forcing (ZF) linear precoding scheme augmented with some appropriately chosen symbol-dependent perturbation terms, and that some extended form of SLP is equivalent to a vector perturbation (VP) nonlinear precoding scheme augmented with the above-noted perturbation terms. We examine how insights arising from this perturbed ZF and VP interpretations can be leveraged to i) substantially simplify the optimization of certain SLP design criteria, namely, total or peak power minimization subject to SEP quality guarantees and under quadrature amplitude modulation (QAM) constellations; and ii) derive heuristic but computationally cheaper SLP designs. We also touch on the analysis side by showing that, under the total power minimization criterion, the basic ZF scheme is a near-optimal SLP scheme when the QAM order is very high—which gives a vital implication that SLP is more useful for lower-order QAM cases. Numerical results further indicate the merits and limitations of the different SLP designs derived from the perturbed ZF and VP interpretations.

1 Introduction

Transmit precoding is a subject that has been studied for decades. It plays a central role in the multiuser multi-input-multi-output (MIMO) scenarios, offering effective transmit signaling schemes to enable spatial multiplexing and to enhance system throughputs. Linear precoding is, by far, the most popular approach: it is easy to realize at the symbol or signal level; it has good design flexibility

to cater for various design needs, such as those from cognitive radio, multi-cell coordination, cell-free MIMO and physical-layer security; and there is a rich line of research concerning how we can design linear precoding for utilitarian throughput maximization, fair throughput allocation, etc.; see, e.g., [1–8]. The decades of transmit precoding research also led to beautiful ideas with nonlinear precoding, such as Tomlinson-Harashima precoding [9] and vector perturbation (VP) precoding [10,11]; they take certain specific modulo-type nonlinear forms and may not be as flexible as linear precoding, but they can greatly improve performance compared to some simple linear precoding schemes such as the zero-forcing (ZF) scheme. In linear precoding we often treat multiuser interference (MUI) as noise, or something to alleviate. However, some recent research argues that MUI is not necessarily adversarial. We can manipulate MUI at the symbol level to help us improve performance. This idea is generally called *symbol-level precoding* (SLP) in the literature.

The currently popular way to define SLP is that we can choose any multi-antenna transmitted signals (absolute freedom rather than a linear form), and the aim is to enhance performance in a symbol-aware fashion, e.g., symbol error probability. For the past decade researchers have been invoking various ideas that gradually evolved to the SLP defined above, and it is worthwhile to briefly recognize such original endeavors. SLP is also known as directional modulation [12–14] and constructive interference (CI) [15–20], depending on the context. In the early 2010, Masouros *et al.* took the intuition that under phase shift keying (PSK) constellations, MUI can be characterized as constructive and destructive [15, 16]. There, the linear precoders are designed such that, at the user side, the CI pushes the received signals deeper into the decision region. Soon, this CI idea was exploited extensively for PSK constellations and in a more general nonlinear form [17, 19, 21–23]. Later, Alodeh *et al.* extended this interference manipulating concept to quadrature amplitude modulation (QAM) constellations [24] and many subsequent works followed this adaptation [20, 25–27]. Lately, SLP has been applied to a number of scenarios, such as MIMO orthogonal frequency division multiplexing [28, 29], physical-layer security [30, 31] and intelligent reflecting surface [32].

In addition to improved symbol-level performance over linear precoding, SLP allows us to have a better control with the transmitted signal amplitudes. Linear precoding, by nature, can only control the average signal amplitudes. The better amplitude control of SLP is particularly beneficial to the recent developments of large-scale or massive MIMO systems. In such systems it is desirable that each antenna is employed with a low-cost radio frequency chain, wherein the power amplifiers trade a smaller linear amplification range for a higher power efficiency. This necessitates the transmitted signals at each antenna to have low amplitude fluctuations at every time instant. SLP has been adopted to deal with more amplitude stringent designs, such as peak-to-average-power ratio minimization [33, 34], constant-envelope precoding [35–37] and one-bit precoding [38–41].

SLP has been extensively employed in a variety of scenarios, as noted above, and the flexibility of SLP as a precoding design framework has been the key factor with its recent prominence. But we see fewer studies that work toward understanding the basic nature of SLP. In particular, the connections between SLP and the existing precoding schemes were relatively under-explored in the prior literature. Researchers somewhat realize that there are connections between SLP and ZF precoding, as indicated in their research; see, e.g., [19, 23, 42]. But the existing literature does not provide a thorough enough investigation on such connections and the subsequent implications on precoding designs.

1.1 This Work and The Contributions

In this paper we study SLP through the lens of ZF and VP precoding. In the conference version of this paper [43], we pointed out that SLP can be equivalently seen as a perturbed ZF scheme. Specifically we inject two perturbation terms, one on the symbols and another on the multiuser channel nullspace, into the ZF scheme; the perturbation terms are symbol-dependent and are the equivalent optimization variables of SLP. That preliminary work also utilized this relationship to design SLP. In the present work we provide a more complete study. We take the classic single-cell multiuser multi-input-single-output (MISO) downlink as our scenario to study the problem, and we consider non-constant modulus QAM constellation cases. Our design criteria of interest are power minimization, either as the total transmission power (TTP) or as the peak per-antenna power (PPAP), subject to constraints that the symbol error probabilities (SEPs) at the user side will meet a pre-determined requirement. As a key result of this paper, we will show that the power reduction gain of SLP over the ZF scheme diminishes as the QAM order increases; the result is based on TTP minimization. Curiously this result suggests that ZF is good enough if we have a very high QAM order. It also answers why we have never seen a numerical result that shows significant performance gains with SLP for very high QAM orders (see, e.g., [24] for numerical results for higher-order QAM). In addition we will show that a modulo-detection extension of SLP can equivalently be seen as a VP scheme with the aforementioned perturbations. Drawing this connection allows us to revisit VP in a new and more general way.

Based on the SLP-ZF and SLP-VP relationships we establish, we investigate how the SLP designs can be facilitated. We will see that, by representing SLP as a perturbed ZF or VP scheme, the SEP constraints are reduced to simple bound constraints. Such structure enables us to build efficient optimization algorithms for our SLP designs. To be more specific, we adopt a fairly general design formulation wherein we optimize SLP over a stream of symbols (typically a few hundreds in length, in practice), and we optimize them jointly with the symbol spacings and rotations at the user side—all for enhanced performance. This leads to a large-scale optimization problem, which, by our experience, cannot be efficiently handled by general-purpose solvers (such as CVX [44]). Fortunately, by exploiting the SLP-ZF or SLP-VP structure, and by solving a subtle technical issue (about projection), we will be able to handle this large-scale problem efficiently by an accelerated projected gradient (APG) algorithm. We will also study suboptimal SLP alternatives for computationally more efficient implementations; they avoid the large-scale problem by some simple intuitive idea.

Our numerical results also reveal useful insights as design guidelines. They will be discussed in the conclusion section after we describe the different SLP designs derived from the SLP-ZF and SLP-VP relationships in the ensuing sections.

1.2 Notations

Our notations are as follows. We use x , \mathbf{x} , \mathbf{X} and \mathcal{X} to denote a scalar, a vector, a matrix and a set, respectively; \mathbb{R} , \mathbb{C} and \mathbb{Z} denote the set of all real numbers, complex numbers and integers, respectively; \mathbf{X}^T , \mathbf{X}^H , \mathbf{X}^{-1} and $\text{Tr}(\mathbf{X})$ are the transpose, Hermitian transpose, inverse and trace of \mathbf{X} , respectively; \mathbf{x}^* stands for the element-wise complex conjugate; $\Re(\mathbf{x})$ and $\Im(\mathbf{x})$ are the real and imaginary components of \mathbf{x} , respectively; \circ denotes the Hadamard product, and \diamond is defined as $\mathbf{x} \diamond \mathbf{y} \triangleq \Re(\mathbf{x}) \circ \Re(\mathbf{y}) + j \Im(\mathbf{x}) \circ \Im(\mathbf{y})$; $\mathbf{x} \geq_c \mathbf{y}$ means $\Re(\mathbf{x}) \geq \Re(\mathbf{y})$ and $\Im(\mathbf{x}) \geq \Im(\mathbf{y})$, where \geq represents the element-wise inequality; $|\mathbf{x}|$ denotes the element-wise modulus of \mathbf{x} ; $\|\mathbf{x}\|_{\mathbf{R}} \triangleq \sqrt{\mathbf{x}^H \mathbf{R} \mathbf{x}}$, where

\mathbf{R} is positive definite, denotes the Mahalanobis norm; $\text{card}(\mathcal{X})$ stands for the cardinality of the set \mathcal{X} ; $\mathcal{CN}(\mu, \sigma^2)$ denotes the circularly symmetric complex Gaussian distribution with mean μ and variance σ^2 .

2 System Model

2.1 Basics

Consider a classic single-cell multiuser MISO downlink scenario, where a base station (BS) with N transmit antennas simultaneously serves K single-antenna users over a frequency-flat block faded channel. The received signal $y_{i,t}$ of the i th user at symbol time t can be modeled by

$$y_{i,t} = \mathbf{h}_i^H \mathbf{x}_t + v_{i,t}, \quad i = 1, \dots, K, \quad t = 1, \dots, T, \quad (1)$$

where $\mathbf{h}_i \in \mathbb{C}^N$ represents the downlink channel from the BS to the i th user; $\mathbf{x}_t \in \mathbb{C}^N$ is the transmitted signal at symbol time t ; $v_{i,t} \sim \mathcal{CN}(0, \sigma_v^2)$ is circular complex Gaussian noise; T is the transmission block length.

Under the above scenario, the goal of precoding is to simultaneously transmit data streams to multiple users, one for each user. To describe, let $s_{i,t}$ be the desired symbol of the i th user at symbol time t . The symbols are assumed to be drawn from a quadrature amplitude modulation (QAM) constellation

$$\mathcal{S} = \{s_R + \mathbf{j}s_I \mid s_R, s_I \in \{\pm 1, \pm 3, \dots, \pm(2L-1)\}\}, \quad (2)$$

where L is a positive integer (the QAM size is $4L^2$), $\mathbf{j} = \sqrt{-1}$. Assuming perfect channel state information at the BS, we aim to design the transmitted signals $\mathbf{x}_1, \dots, \mathbf{x}_T$ such that the users will receive their desired symbols, subject to certain scalings and rotations. Specifically, as illustrated in Fig. 1, we want the noise-free part of $y_{i,t}$ in (1) to take the form

$$\begin{aligned} \mathbf{h}_i^H \mathbf{x}_t &\approx \varphi_i(d_i^R \Re(s_{i,t}) + \mathbf{j}d_i^I \Im(s_{i,t})) \\ &= \varphi_i(d_i \diamond s_{i,t}), \quad i = 1, \dots, K, \quad t = 1, \dots, T, \end{aligned} \quad (3)$$

where $\varphi_i = e^{\mathbf{j}\theta_i}$, $\theta_i \in [0, 2\pi]$, describes the phase rotation of the QAM constellation for the i th user; $d_i^R \geq 0$ and $d_i^I \geq 0$ are the half inter-symbol spacings of the real and imaginary components of the QAM constellation for the i th user, respectively; $d_i = d_i^R + \mathbf{j}d_i^I$. For the sake of notational conciseness, we will also write (3) as

$$\mathbf{H}\mathbf{x}_t \approx \boldsymbol{\varphi} \circ (\mathbf{d} \diamond \mathbf{s}_t), \quad t = 1, \dots, T, \quad (4)$$

where $\mathbf{H} = [\mathbf{h}_1, \dots, \mathbf{h}_K]^H$, $\boldsymbol{\varphi} = [\varphi_1, \dots, \varphi_K]^T$, $\mathbf{d} = [d_1, \dots, d_K]^T$ and $\mathbf{s}_t = [s_{1,t}, \dots, s_{K,t}]^T$. The attempt of making a good approximation of (3) or (4) will be called *symbol shaping* in the sequel.

Some basic aspects should be mentioned. The half inter-symbol spacings d_i 's and phase rotations φ_i 's are to be designed, as will be elucidated later. Throughout this paper we assume that each user knows its corresponding d_i and θ_i , which can be obtained by channel estimation during the training phase.

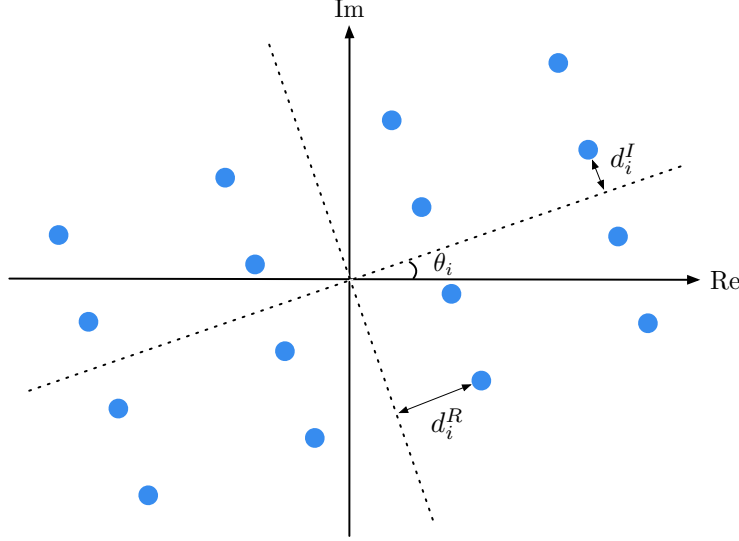


Figure 1: Illustration of d_i and θ_i for 16-QAM constellation.

2.2 Linear Precoding

To provide intuition, we first review how linear precoding performs symbol shaping. In linear precoding, the transmitted signal \mathbf{x}_t takes the form

$$\mathbf{x}_t = \sum_{i=1}^K \mathbf{w}_i s_{i,t}, \quad (5)$$

where $\mathbf{w}_i \in \mathbb{C}^N$ is the precoding or beamforming vector of the i th user. The noise-free part of the received signal $y_{i,t}$ is then given by

$$\mathbf{h}_i^H \mathbf{x}_t = \mathbf{h}_i^H \mathbf{w}_i s_{i,t} + \sum_{j \neq i} \mathbf{h}_i^H \mathbf{w}_j s_{i,t},$$

where $\mathbf{h}_i^H \mathbf{w}_i s_{i,t}$ is the desired symbol scaled by $\mathbf{h}_i^H \mathbf{w}_i$, and $\sum_{j \neq i} \mathbf{h}_i^H \mathbf{w}_j s_{i,t}$ is the multiuser interference (MUI). In linear precoding, the MUI is often treated as Gaussian noise. Also, the beamforming vectors are typically designed to maximize some utility defined over a certain quality-of-service (QoS) metric, e.g., the signal-to-interference-and-noise ratio (SINR)

$$\text{SINR}_i = \frac{\rho |\mathbf{h}_i^H \mathbf{w}_i|^2}{\sum_{j \neq i} \rho |\mathbf{h}_i^H \mathbf{w}_j|^2 + \sigma_v^2},$$

where $\rho = \mathbb{E}[|s_{i,t}|^2]$ is the average symbol power; or, power minimization under some target QoS requirements is sought. The reader is referred to the literature [1–8] and the references therein for details. Such QoS metric often ignores the constellation structure; the SINR defined above is an example. On the other hand, from the perspective of symbol shaping in (3), we see the MUI $\sum_{j \neq i} \mathbf{h}_i^H \mathbf{w}_j s_{i,t}$ as an approximation error, $\varphi_i = e^{j\angle(\mathbf{h}_i^H \mathbf{w}_i)}$ as the phase rotation, and $d_i = (1 + j)|\mathbf{h}_i^H \mathbf{w}_i|$ as the half inter-symbol spacing.

2.3 SLP and Symbol-Error Probability Characterization

Symbol-level precoding (SLP) attains symbol shaping by allowing the transmitted signal \mathbf{x}_t to take any form. It also utilizes the constellation structure. To put into context, consider the symbol-error probability (SEP) as our QoS metric. Assume that the users detect the symbols by the standard decision rule

$$\hat{s}_{i,t} = \text{dec}\left(\frac{\Re(\varphi_i^* y_{i,t})}{d_i^R}\right) + \mathbf{j} \cdot \text{dec}\left(\frac{\Im(\varphi_i^* y_{i,t})}{d_i^I}\right), \quad (6)$$

where $\text{dec}(\cdot)$ denotes the decision function corresponding to $\{\pm 1, \pm 3, \dots, \pm(2L-1)\}$. We are interested in

$$\text{SEP}_{i,t} \triangleq \Pr(\hat{s}_{i,t} \neq s_{i,t} \mid s_{i,t}) \leq \varepsilon_i, \quad (7)$$

for a given SEP target $\varepsilon_i > 0$. A sufficient condition for (7) to hold is as follows.

Fact 1 *The SEP constraints in (7) hold for all i if*

$$-\mathbf{d} + \mathbf{a}_t \leq_c \varphi^* \circ (\mathbf{H} \mathbf{x}_t) - \mathbf{d} \diamond \mathbf{s}_t \leq_c \mathbf{d} - \mathbf{c}_t, \quad (8)$$

where $\mathbf{a}_t = [a_{1,t}, \dots, a_{K,t}]^T$, $a_{i,t} = a_{i,t}^R + \mathbf{j} a_{i,t}^I$, $\mathbf{c}_t = [c_{1,t}, \dots, c_{K,t}]^T$, $c_{i,t} = c_{i,t}^R + \mathbf{j} c_{i,t}^I$;

$$\begin{aligned} a_{i,t}^R &= \begin{cases} \alpha_i, & |\Re(s_{i,t})| < 2L-1 \\ \beta_i, & \Re(s_{i,t}) = 2L-1 \\ -\infty, & \Re(s_{i,t}) = -2L+1 \end{cases} \\ c_{i,t}^R &= \begin{cases} \alpha_i, & |\Re(s_{i,t})| < 2L-1 \\ -\infty, & \Re(s_{i,t}) = 2L-1 \\ \beta_i, & \Re(s_{i,t}) = -2L+1 \end{cases} \end{aligned} \quad (9)$$

and

$$\alpha_i = \frac{\sigma_u}{\sqrt{2}} Q^{-1}\left(\frac{1-\sqrt{1-\varepsilon_i}}{2}\right), \quad \beta_i = \frac{\sigma_u}{\sqrt{2}} Q^{-1}(1 - \sqrt{1-\varepsilon_i}); \quad (10)$$

$a_{i,t}^I$ and $c_{i,t}^I$ are defined the same as $a_{i,t}^R$ and $c_{i,t}^R$ in (9) by replacing “ R ” with “ I ” and “ \Re ” with “ \Im ”.

The derivations leading to Fact 1 are as follows. Let

$$\begin{aligned} \text{SEP}_{i,t}^R &= \Pr(\Re(\hat{s}_{i,t}) \neq \Re(s_{i,t}) \mid s_{i,t}), \\ \text{SEP}_{i,t}^I &= \Pr(\Im(\hat{s}_{i,t}) \neq \Im(s_{i,t}) \mid s_{i,t}), \end{aligned}$$

which are the error probabilities with the real and imaginary components of $\hat{s}_{i,t}$, respectively. It is easy to verify that

$$\text{SEP}_{i,t}^R \leq 1 - \sqrt{1-\varepsilon_i}, \quad \text{SEP}_{i,t}^I \leq 1 - \sqrt{1-\varepsilon_i} \Rightarrow \text{SEP}_{i,t} \leq \varepsilon_i. \quad (11)$$

Also, it is known from [40, 43] that

$$\begin{aligned}\text{SEP}_{i,t}^R &= Q\left(\frac{\sqrt{2}}{\sigma_v}(d_i^R - b_{i,t}^R)\right) + Q\left(\frac{\sqrt{2}}{\sigma_v}(d_i^R + b_{i,t}^R)\right) \\ &\leq 2Q\left(\frac{\sqrt{2}}{\sigma_v}(d_i^R - |b_{i,t}^R|)\right), \quad |\Re(s_{i,t})| < 2L - 1, \\ \text{SEP}_{i,t}^R &= Q\left(\frac{\sqrt{2}}{\sigma_v}(d_i^R + b_{i,t}^R)\right), \quad \Re(s_{i,t}) = 2L - 1, \\ \text{SEP}_{i,t}^R &= Q\left(\frac{\sqrt{2}}{\sigma_v}(d_i^R - b_{i,t}^R)\right), \quad \Re(s_{i,t}) = -2L + 1,\end{aligned}$$

where $Q(x) = \int_x^\infty \frac{1}{\sqrt{2\pi}} e^{-z^2/2} dz$;

$$b_{i,t}^R = \Re(\varphi_i^* \mathbf{h}_i^H \mathbf{x}_t) - d_i^R \Re(s_{i,t}).$$

Since $Q(\cdot)$ is monotone decreasing, we have

$$-d_i^R + a_{i,t}^R \leq \Re(\varphi_i^* \mathbf{h}_i^H \mathbf{x}_t) - d_i^R \Re(s_{i,t}) \leq d_i^R - c_{i,t}^R \Rightarrow \text{SEP}_{i,t}^R \leq 1 - \sqrt{1 - \varepsilon_i}. \quad (12)$$

Similarly, the result in (12) also holds for $\text{SEP}_{i,t}^I$ by replacing “ R ” with “ I ” and “ \Re ” with “ \Im ”.

3 A New Look at SLP

In this section, we introduce a new way to represent SLP, which will enable us to link SLP with linear precoding.

3.1 Precoding via the Lens of Zero-Forcing

Let us make an assumption that is arguably standard in multiuser MISO channels:

Assumption 1 *The channel matrix \mathbf{H} has full row rank.*

The following result will be important in our subsequent developments.

Fact 2 *Suppose that Assumption 1 holds. Let $\mathbf{s}_t \in \mathbb{C}^K$, $\mathbf{d} \in \mathbb{C}^K$ and $\varphi \in \mathbb{C}^K$ with $|\varphi| = 1$, be given. Any $\mathbf{x}_t \in \mathbb{C}^N$ can be represented by*

$$\mathbf{x}_t = \mathbf{H}^\dagger(\varphi \circ (\mathbf{d} \diamond \mathbf{s}_t + \mathbf{u}_t)) + \mathbf{B}\mathbf{z}_t, \quad (13)$$

for some $\mathbf{u}_t \in \mathbb{C}^K$ and $\mathbf{z}_t \in \mathbb{C}^{N-K}$, where $\mathbf{H}^\dagger \triangleq \mathbf{H}^H(\mathbf{H}\mathbf{H}^H)^{-1}$ is the pseudo-inverse of \mathbf{H} , and $\mathbf{B} \in \mathbb{C}^{N \times (N-K)}$ is a basis matrix for the nullspace of \mathbf{H} . Also, under the representation (13), we can equivalently represent the SEP quality guarantee (8) in Fact 1 by

$$-\mathbf{d} + \mathbf{a}_t \leq_c \mathbf{u}_t \leq_c \mathbf{d} - \mathbf{c}_t. \quad (14)$$

Proof: Let $\mathcal{R} \subseteq \mathbb{C}^N$ denote the range space of \mathbf{H}^H . Let \mathcal{R}^\perp be the orthogonal complement of \mathcal{R} , which is also the nullspace of \mathbf{H} . Any $\mathbf{x}_t \in \mathbb{C}^N$ can be decomposed into $\mathbf{x}_t = \bar{\mathbf{x}}_t + \tilde{\mathbf{x}}_t$, where $\bar{\mathbf{x}}_t \in \mathcal{R}$ and $\tilde{\mathbf{x}}_t \in \mathcal{R}^\perp$. By letting \mathbf{B} be a basis matrix for \mathcal{R}^\perp , we can represent $\tilde{\mathbf{x}}_t$ by $\tilde{\mathbf{x}}_t = \mathbf{B}\mathbf{z}_t$ for some \mathbf{z}_t . In the same vein, we can write $\bar{\mathbf{x}}_t = \mathbf{H}^H \mathbf{r}_t$ for some \mathbf{r}_t . Let $\mathbf{s}_t, \mathbf{d}, \varphi$ ($|\varphi| = 1$) be given. Choose \mathbf{u}_t such that

$$\mathbf{r}_t = (\mathbf{H}\mathbf{H}^H)^{-1}(\varphi \circ (\mathbf{d} \diamond \mathbf{s}_t + \mathbf{u}_t)), \quad (15)$$

or equivalently,

$$\mathbf{u}_t = \varphi^* \circ (\mathbf{H}\mathbf{H}^H \mathbf{r}_t) - \mathbf{d} \diamond \mathbf{s}_t.$$

Putting (15), $\bar{\mathbf{x}}_t = \mathbf{H}^H \mathbf{r}_t$ and $\tilde{\mathbf{x}}_t = \mathbf{B}\mathbf{z}_t$ into $\mathbf{x}_t = \bar{\mathbf{x}}_t + \tilde{\mathbf{x}}_t$ gives the representation in (13). Furthermore, putting (13) into (8) gives the result in (14). \blacksquare

Fact 2 shows two key revelations. Firstly, an SLP scheme is equivalent to a zero-forcing (ZF) scheme with a symbol perturbation \mathbf{u}_t and a nullspace perturbation $\mathbf{B}\mathbf{z}_t$. From that point of view we can regard SLP as instances of ZF, with suitable perturbations. The most obvious one is the traditional ZF scheme $\mathbf{x}_t^{\text{ZF}} = \mathbf{H}^\dagger(\mathbf{d} \diamond \mathbf{s}_t)$ itself, which is an instance of (13) with $\mathbf{u}_t = \mathbf{0}$, $\mathbf{z}_t = \mathbf{0}$ and $\varphi = 1$. Secondly, we see from (14) that the SEP quality guarantee (8) depends only on the symbol perturbation component \mathbf{u}_t and the half inter-symbol spacing \mathbf{d} . This result will substantially simplify our designs.

3.2 SLP is Symbol-Perturbed ZF

Consider an SLP design that minimizes the total transmission power (TTP) under the SEP quality guarantee in (8):

$$\begin{aligned} & \min_{\mathbf{d}, \varphi, \mathbf{X}} \frac{1}{T} \sum_{t=1}^T \|\mathbf{x}_t\|_2^2 \\ & \text{s.t. } -\mathbf{d} + \mathbf{a}_t \leq_c \varphi^* \circ (\mathbf{H}\mathbf{x}_t) - \mathbf{d} \diamond \mathbf{s}_t \leq_c \mathbf{d} - \mathbf{c}_t, \quad t = 1, \dots, T, \\ & \quad \mathbf{d} \geq_c \mathbf{0}, \quad |\varphi| = 1, \end{aligned} \quad (16)$$

where $\mathbf{X} = [\mathbf{x}_1, \dots, \mathbf{x}_T]$. The SLP problem (16) designs not only the transmitted signals \mathbf{x}_t 's but also the half inter-symbol spacings d_t 's and the phase rotations φ_t 's to best optimize the TTP. Using the alternative SLP representation in Fact 2, we have the following result.

Proposition 1 Suppose that Assumption 1 holds. Then an optimal $\mathbf{X}^* = [\mathbf{x}_1^*, \dots, \mathbf{x}_T^*]$ to Problem (16) is given by

$$\mathbf{x}_t^* = \mathbf{H}^\dagger(\varphi^* \circ (\mathbf{d}^* \diamond \mathbf{s}_t + \mathbf{u}_t^*)), \quad t = 1, \dots, T,$$

where $(\mathbf{d}^*, \varphi^*, \mathbf{U}^*)$, $\mathbf{U}^* = [\mathbf{u}_1^*, \dots, \mathbf{u}_T^*]$, is an optimal solution to

$$\begin{aligned} & \min_{\mathbf{d}, \varphi, \mathbf{U}} \frac{1}{T} \sum_{t=1}^T \|\mathbf{d} \diamond \mathbf{s}_t + \mathbf{u}_t\|_{\mathbf{R}_\varphi}^2 \\ & \text{s.t. } -\mathbf{d} + \mathbf{a}_t \leq_c \mathbf{u}_t \leq_c \mathbf{d} - \mathbf{c}_t, \quad t = 1, \dots, T, \\ & \quad \mathbf{d} \geq_c \mathbf{0}, \quad |\varphi| = 1, \end{aligned} \quad (17)$$

with $\mathbf{R}_\varphi = \text{Diag}(\varphi)^H \mathbf{R} \text{Diag}(\varphi)$ and $\mathbf{R} = (\mathbf{H}\mathbf{H}^H)^{-1}$.

Proof: Substituting (13) into Problem (16) gives

$$\begin{aligned} \min_{\mathbf{d}, \boldsymbol{\varphi}, \{\mathbf{u}_t, \mathbf{z}_t\}_{t=1}^T} \quad & \frac{1}{T} \sum_{t=1}^T (\|\mathbf{d} \diamond \mathbf{s}_t + \mathbf{u}_t\|_{\mathbf{R}_{\boldsymbol{\varphi}}}^2 + \|\mathbf{B}\mathbf{z}_t\|_2^2) \\ \text{s.t.} \quad & -\mathbf{d} + \mathbf{a}_t \leq_c \mathbf{u}_t \leq_c \mathbf{d} - \mathbf{c}_t, \quad t = 1, \dots, T, \\ & \mathbf{d} \geq_c \mathbf{0}, \quad |\boldsymbol{\varphi}| = 1. \end{aligned}$$

We see that any optimal solution to the above problem must have $\|\mathbf{B}\mathbf{z}_t\|_2^2 = 0$, or equivalently, $\mathbf{z}_t = \mathbf{0}$, for all t . The proof is complete. \blacksquare

Proposition 1 indicates that the optimal SLP scheme under the TTP minimization design (16) is a symbol-perturbed ZF scheme, with the nullspace components being shut down. Also, the equivalent TTP minimization problem (17) appears to be easier to deal with than its original counterpart (16); the constraints for \mathbf{u}_t and \mathbf{d} in Problem (17) are simple bound inequalities, while their counterparts in Problem (16) are linearly mixed inequalities with respect to (w.r.t.) \mathbf{X} and \mathbf{d} .

3.3 ZF is a Near-Optimal SLP for Very Large QAM Sizes

We showed in the preceding subsection that the optimal SLP scheme under the TTP minimization design (16) is a symbol-perturbed ZF scheme. In fact, we can even show that the optimal SLP scheme reduces to the basic ZF scheme—without symbol perturbations—under certain assumptions. Let us set the stage by assuming the following:

Assumption 2 *The QAM order L (cf. (2)) has $L \geq 2$; i.e., non-constant modulus QAM cases. Each user's symbol stream $s_{i,1}, \dots, s_{i,T}$ has at least one symbol $s_{i,t}$ such that $|\Re(s_{i,t})| < 2L - 1$ and $|\Im(s_{i,t})| < 2L - 1$; that is, $s_{i,t}$ is an inner constellation point (ICP) of the QAM constellation.*

Assumption 3 *The symbols $s_{i,t}$'s are independently and identically distributed (i.i.d.) and are uniformly distributed on the QAM constellation \mathcal{S} .*

Assumption 4 *The transmission block length T tends to infinity.*

The SLP design problem (17) under Assumptions 1–4 can be written as

$$f_{\text{SLP}} = \min_{\mathbf{d} \geq_c \boldsymbol{\alpha}_c, |\boldsymbol{\varphi}|=1} g(\mathbf{d}, \boldsymbol{\varphi}), \quad (18)$$

where $\boldsymbol{\alpha}_c \triangleq \boldsymbol{\alpha} + \mathbf{j}\boldsymbol{\alpha}$ ($\boldsymbol{\alpha}$ was defined in (10)),

$$g(\mathbf{d}, \boldsymbol{\varphi}) = \mathbb{E}_{\mathbf{s}_t} \left[\min_{\mathbf{u}_t \in \mathcal{U}(\mathbf{s}_t, \mathbf{d})} \|\mathbf{d} \diamond \mathbf{s}_t + \mathbf{u}_t\|_{\mathbf{R}_{\boldsymbol{\varphi}}}^2 \right],$$

$\mathcal{U}(\mathbf{s}_t, \mathbf{d}) = \mathcal{U}(s_{1,t}, d_1) \times \dots \times \mathcal{U}(s_{K,t}, d_K)$ with $\mathcal{U}(s_{i,t}, d_i) \triangleq \{u_i \in \mathbb{C} \mid -d_i + a_{i,t} \leq_c u_i \leq_c d_i - c_{i,t}\}$. Note that we replace $\mathbf{d} \geq_c \mathbf{0}$ with $\mathbf{d} \geq_c \boldsymbol{\alpha}_c$, and this is without loss of generality because one can show that $\mathbf{d} \geq_c \boldsymbol{\alpha}_c$ must hold under Assumption 2¹. Let

$$\mathbf{x}_t^{\text{ZF}} = \mathbf{H}^\dagger(\boldsymbol{\alpha}_c \diamond \mathbf{s}_t), \quad (19)$$

¹The proof is as follows. From (8) we must have $-d_i + a_{i,t} \leq_c d_i - c_{i,t}$, or equivalently, $d_i \geq_c (a_{i,t} + c_{i,t})/2$, for all i, t . Let $s_{i,t}$ be an ICP. By $a_{i,t} = c_{i,t} = \alpha_i + \mathbf{j}\alpha_i$ (see (9)), we get $d_i \geq_c \alpha_i + \mathbf{j}\alpha_i$.

be our benchmark ZF scheme where $\mathbf{d} = \boldsymbol{\alpha}_c$, $\boldsymbol{\varphi} = \mathbf{1}$ and $\mathbf{u}_t = \mathbf{0}$. Note that the ZF scheme (19) satisfies the SEP quality guarantee (8) since it is a feasible solution to Problem (18). Our result is as follows.

Theorem 1 *Suppose that Assumptions 1–4 hold. Also, suppose that $\varepsilon_1 = \dots = \varepsilon_K = \varepsilon$. Then the optimal value f_{SLP} of Problem (18) satisfies*

$$\kappa f_{\text{ZF}} \leq f_{\text{SLP}} \leq f_{\text{ZF}},$$

where $f_{\text{ZF}} = \mathbb{E}_{\mathbf{s}_t} [\|\mathbf{x}_t^{\text{ZF}}\|_2^2]$ is the (average) TTP of ZF, and

$$\kappa = \left(1 - \frac{1}{L}\right)^{2K} \frac{2L-3}{2L+1} \frac{(2L-1)(2L-3)-3}{(2L-1)(2L-3)-3 + \frac{3\lambda_{\max}(\mathbf{R})}{\lambda_{\min}(\mathbf{R})}}.$$

The proof of Theorem 1 will be described in the next subsection. Theorem 1 suggests that the TTP ratio between SLP and ZF is lower bounded by κ ($\kappa < 1$). In particular, κ increases as L increases, and $\kappa \rightarrow 1$ as $L \rightarrow \infty$. This leads to the following important conclusion:

Corollary 1 *Under Assumptions 1–4, the optimal SLP scheme under the TTP minimization design (17) approaches the ZF scheme (19) as the QAM size tends to infinity.*

Corollary 1 suggests that, for very high-order QAM, we may simply use ZF. Our numerical results will illustrate that the ZF scheme is indeed near-optimal for very large L . On the other hand, our numerical results will also indicate that, for smaller L , the optimal SLP scheme and its variant (to be described) can have significant TTP reduction over the ZF scheme.

3.4 Proof of Theorem 1

We first prove $f_{\text{SLP}} \leq f_{\text{ZF}}$. As the ZF scheme (19) is feasible to Problem (18), we have

$$f_{\text{SLP}} \leq \mathbb{E}_{\mathbf{s}_t} \left[\|\mathbf{x}_t^{\text{ZF}}\|_2^2 \right] = \mathbb{E}_{\mathbf{s}_t} \left[\|\boldsymbol{\alpha}_c \diamond \mathbf{s}_t\|_{\mathbf{R}}^2 \right] = \alpha^2 \rho \text{Tr}(\mathbf{R}).$$

Note that the last equation above is due to $\mathbb{E}[s_{i,t}^* s_{j,t}] = 0$ for $i \neq j$ and $\mathbb{E}[|s_{i,t}|^2] = \rho$. Next, we prove $\kappa f_{\text{ZF}} \leq f_{\text{SLP}}$. The following two lemmas will be required, and their proofs are shown in the Appendixes A-B.

Lemma 1 *Consider*

$$p^* = \min_{\mathbf{x} \in \mathbb{C}^K} \|\mathbf{x} + \mathbf{b}\|_{\mathbf{A}}^2 \quad \text{s.t. } -\mathbf{c} \leq_c \mathbf{x} \leq_c \mathbf{c}, \quad (20)$$

where \mathbf{A} is Hermitian positive definite. Then, for any $\beta \geq 0$, we have

$$p^* \geq \mathbf{b}^H (\mathbf{A} - \mathbf{A}(\mathbf{A} + \beta \mathbf{I})^{-1} \mathbf{A}) \mathbf{b} - \beta \|\mathbf{c}\|_2^2.$$

Lemma 2 *Suppose \mathbf{R} is Hermitian positive definite.*

(a) *For any $|\boldsymbol{\varphi}| = \mathbf{1}$, $\mathbf{R}_{\boldsymbol{\varphi}} \triangleq \text{Diag}(\boldsymbol{\varphi})^H \mathbf{R} \text{Diag}(\boldsymbol{\varphi})$ and \mathbf{R} share the same eigenvalues.*

(b) Let $\tilde{\mathbf{R}}_{\varphi} = \mathbf{R}_{\varphi} - \mathbf{R}_{\varphi}(\mathbf{R}_{\varphi} + \beta\mathbf{I})^{-1}\mathbf{R}_{\varphi}$ where $\beta \geq 0$. We have

$$\lambda_i(\tilde{\mathbf{R}}_{\varphi}) = \frac{\lambda_i(\mathbf{R})\beta}{\lambda_i(\mathbf{R}) + \beta}, \quad \forall i, \quad (21)$$

where $\lambda_i(\mathbf{X})$ denotes the i th largest eigenvalue of \mathbf{X} .

Firstly, we derive a lower bound for $g(\mathbf{d}, \varphi)$. Denote \mathcal{I} as the set of all ICPs of \mathcal{S} , and let $\mathcal{D}_{\mathcal{I}}$ be the uniform distribution on \mathcal{I} . It holds that, for any $\beta \geq 0$,

$$\begin{aligned} g(\mathbf{d}, \varphi) &= \frac{1}{(2L)^{2K}} \sum_{\mathbf{s}_t \in \mathcal{S}^K} \left[\min_{\mathbf{u}_t \in \mathcal{U}(\mathbf{s}_t, \mathbf{d})} \|\mathbf{d} \diamond \mathbf{s}_t + \mathbf{u}_t\|_{\mathbf{R}_{\varphi}}^2 \right] \\ &\geq \frac{1}{(2L)^{2K}} \sum_{\mathbf{s}_t \in \mathcal{I}^K} \left[\min_{-\mathbf{d} + \boldsymbol{\alpha}_c \leq_c \mathbf{u}_t \leq_c \mathbf{d} - \boldsymbol{\alpha}_c} \|\mathbf{d} \diamond \mathbf{s}_t + \mathbf{u}_t\|_{\mathbf{R}_{\varphi}}^2 \right] \\ &= \left(1 - \frac{1}{L}\right)^{2K} \mathbb{E}_{\mathbf{s}_t \sim \mathcal{D}_{\mathcal{I}}^K} \left[\min_{-\mathbf{d} + \boldsymbol{\alpha}_c \leq_c \mathbf{u}_t \leq_c \mathbf{d} - \boldsymbol{\alpha}_c} \|\mathbf{d} \diamond \mathbf{s}_t + \mathbf{u}_t\|_{\mathbf{R}_{\varphi}}^2 \right] \\ &\geq \left(1 - \frac{1}{L}\right)^{2K} \mathbb{E}_{\mathbf{s}_t \sim \mathcal{D}_{\mathcal{I}}^K} \left[(\mathbf{d} \diamond \mathbf{s}_t)^H \tilde{\mathbf{R}}_{\varphi} (\mathbf{d} \diamond \mathbf{s}_t) \right] - \beta \|\mathbf{d} - \boldsymbol{\alpha}_c\|_2^2 \\ &= \left(1 - \frac{1}{L}\right)^{2K} \sum_{i=1}^K \left(\frac{\bar{\rho}}{2} \tilde{r}_{\varphi, i} |d_i|^2 - \beta |d_i - \alpha_c|^2 \right), \end{aligned} \quad (22)$$

where $\tilde{\mathbf{R}}_{\varphi} = \mathbf{R}_{\varphi} - \mathbf{R}_{\varphi}(\mathbf{R}_{\varphi} + \beta\mathbf{I})^{-1}\mathbf{R}_{\varphi}$; $\bar{\rho} = \mathbb{E}_{s_{i,t} \sim \mathcal{D}_{\mathcal{I}}} [|s_{i,t}|^2]$; $\tilde{r}_{\varphi, i}$ is the (i, i) th entry of $\tilde{\mathbf{R}}_{\varphi}$; the second equation is due to $\mathcal{I} \subset \mathcal{S}$; the fourth equation follows from Lemma 1.

Secondly, we specify the choice of $\beta \geq 0$ to obtain the desired result. Plugging (22) into (18) gives

$$f_{\text{SLP}} \geq \left(1 - \frac{1}{L}\right)^{2K} \min_{\substack{\mathbf{d} \geq_c \boldsymbol{\alpha}_c, \\ |\varphi| = \mathbf{1}}} \sum_{i=1}^K \left(\frac{\bar{\rho}}{2} \tilde{r}_{\varphi, i} |d_i|^2 - \beta |d_i - \alpha_c|^2 \right). \quad (23)$$

Observe from (23) that, given any $|\varphi| = \mathbf{1}$, the optimization over \mathbf{d} is decoupled for each d_i , i.e.,

$$\min_{d_i \geq_c \alpha_c} \left(\frac{\bar{\rho}}{2} \tilde{r}_{\varphi, i} |d_i|^2 - \beta |d_i - \alpha_c|^2 \right), \quad (24)$$

which is a one-dimensional quadratic program. We choose $\beta = (\bar{\rho}/2 - 1)\lambda_{\min}(\mathbf{R})$. It can be shown that the optimal solution to Problem (24) is $d_i = \alpha_c$. As a result,

$$\begin{aligned} &\min_{\substack{\mathbf{d} \geq_c \boldsymbol{\alpha}_c, \\ |\varphi| = \mathbf{1}}} \sum_{i=1}^K \left(\frac{\bar{\rho}}{2} \tilde{r}_{\varphi, i} |d_i|^2 - \beta |d_i - \alpha_c|^2 \right) \\ &= \frac{\bar{\rho}}{2} |\alpha_c|^2 \min_{|\varphi| = \mathbf{1}} \sum_{i=1}^K \tilde{r}_{\varphi, i} \\ &= \frac{\bar{\rho}}{2} |\alpha_c|^2 \sum_{i=1}^K \lambda_i(\tilde{\mathbf{R}}_{\varphi}) \\ &\geq \frac{\bar{\rho}}{2} |\alpha_c|^2 \frac{(\frac{\bar{\rho}}{2} - 1)\lambda_{\min}(\mathbf{R})}{\lambda_{\max}(\mathbf{R}) + (\frac{\bar{\rho}}{2} - 1)\lambda_{\min}(\mathbf{R})} \sum_{i=1}^K \lambda_i(\mathbf{R}), \end{aligned} \quad (25)$$

where the second equality is due to Lemma 2(a); the last inequality is due to Lemma 2(b) and $\lambda_i(\mathbf{R}) \leq \lambda_{\max}(\mathbf{R})$ for all i . By invoking

$$\rho = \frac{2(2L+1)(2L-1)}{3}, \quad \bar{\rho} = \frac{2(2L-1)(2L-3)}{3},$$

$\sum_{i=1}^K \lambda_i(\mathbf{R}) = \text{Tr}(\mathbf{R})$, and by plugging (25) into (23), we get $\kappa f_{\text{ZF}} \leq f_{\text{SLP}}$. This completes the proof.

4 SLP Schemes for TTP Minimization

We now turn to solving the TTP minimization SLP design (17). Let us recapitulate Problem (17):

$$\begin{aligned} \min_{\mathbf{d}, \mathbf{U}, \varphi} \quad & f_{\text{TTP}}(\mathbf{d}, \mathbf{U}, \varphi) \triangleq \frac{1}{T} \sum_{t=1}^T \|\mathbf{d} \diamond \mathbf{s}_t + \mathbf{u}_t\|_{\mathbf{R}_\varphi}^2 \\ \text{s.t.} \quad & -\mathbf{d} + \mathbf{a}_t \leq_c \mathbf{u}_t \leq_c \mathbf{d} - \mathbf{c}_t, \quad t = 1, \dots, T, \\ & \mathbf{d} \geq_c \boldsymbol{\alpha}_c, \quad |\varphi| = 1. \end{aligned} \quad (26)$$

Note that we change $\mathbf{d} \geq_c \mathbf{0}$ to $\mathbf{d} \geq_c \boldsymbol{\alpha}_c$ in (26), which is without loss under Assumption 2 as we explained in Problem (18) in Section 3.3. We should briefly mention the problem nature. Problem (26) is a large-scale problem since T is large in practice, say, a few hundreds. The objective function of (26) is convex with respect to w.r.t. either φ or (\mathbf{d}, \mathbf{U}) , but not w.r.t. both. Also, the unit-modulus constraint $|\varphi| = 1$ is non-convex.

4.1 Alternating Minimization over (\mathbf{d}, \mathbf{U}) and φ

We tackle Problem (26) by alternating minimization (AM) over (\mathbf{d}, \mathbf{U}) and φ . At the $(k+1)$ th AM iteration, we compute

$$\begin{aligned} \varphi^{k+1} & \in \arg \min_{|\varphi|=1} f_{\text{TTP}}(\mathbf{d}^k, \mathbf{U}^k, \varphi), \\ (\mathbf{d}^{k+1}, \mathbf{U}^{k+1}) & \in \arg \min_{(\mathbf{d}, \mathbf{U}) \in \mathcal{X}} f_{\text{TTP}}(\mathbf{d}, \mathbf{U}, \varphi^{k+1}), \end{aligned} \quad (27)$$

where

$$\mathcal{X} \triangleq \{(\mathbf{d}, \mathbf{U}) \mid -\mathbf{d} + \mathbf{a}_t \leq_c \mathbf{u}_t \leq_c \mathbf{d} - \mathbf{c}_t, \quad t = 1, \dots, T, \quad \mathbf{d} \geq_c \boldsymbol{\alpha}_c\}.$$

Let us describe how the above minimizations are handled. First, given (\mathbf{d}, \mathbf{U}) , the minimization of f_{TTP} in (26) over φ can be shown to be

$$\min_{\varphi} \varphi^H \bar{\mathbf{R}} \varphi, \quad \text{s.t. } |\varphi| = 1, \quad (28)$$

where $\bar{\mathbf{R}} \triangleq \frac{1}{T} \sum_{t=1}^T \text{Diag}(\mathbf{d} \diamond \mathbf{s}_t + \mathbf{u}_t)^H \mathbf{R} \text{Diag}(\mathbf{d} \diamond \mathbf{s}_t + \mathbf{u}_t)$. Problem (28) is an instance of the unit-modulus quadratic program. Although the unit-modulus quadratic program is non-convex, in practice there are efficient methods that can approximate the problem well, such as semidefinite relaxation [45] and the projected gradient (PG) method [46, 47]. We choose the PG method to handle Problem (28), and the details are relegated to the supplemental material.

Second, given φ , the minimization of f_{TPP} over (\mathbf{d}, \mathbf{U})

$$\begin{aligned} \min_{\mathbf{d}, \mathbf{U}} \phi(\mathbf{d}, \mathbf{U}) &\triangleq \frac{1}{T} \sum_{t=1}^T \|\mathbf{d} \diamond \mathbf{s}_t + \mathbf{u}_t\|_{\mathbf{R}_\varphi}^2 \\ \text{s.t. } -\mathbf{d} + \mathbf{a}_t &\leq_c \mathbf{u}_t \leq_c \mathbf{d} - \mathbf{c}_t, \quad t = 1, \dots, T, \\ \mathbf{d} &\geq_c \boldsymbol{\alpha}_c \end{aligned} \tag{29}$$

is a convex quadratic program subject to linear constraints. However, the constraints are coupled due to the half inter-symbol spacing \mathbf{d} . This, together with the fact that T is large, makes Problem (29) a large-scale problem. Using general-purpose convex optimization software (such as CVX [44]) to solve Problem (29) is no different from treating Problem (29) as a general and unstructured quadratic program, and is computationally prohibitive as we found out. We custom-build a first-order method, namely, the accelerated projected gradient (APG) method [48], to solve Problem (29), in which we exploit the constraint structure for efficient implementations.

To describe the APG method, denote $\boldsymbol{\xi} \triangleq (\mathbf{d}, \mathbf{U})$ and write Problem (29) in a standard optimization form

$$\min_{\boldsymbol{\xi}} \phi(\boldsymbol{\xi}), \quad \text{s.t. } \boldsymbol{\xi} \in \mathcal{X}. \tag{30}$$

The APG updates for Problem (30) are given by

$$\begin{aligned} \boldsymbol{\xi}^{l+1} &= \Pi_{\mathcal{X}}(\mathbf{p}^l - \eta_l \nabla \phi(\mathbf{p}^l)), \\ \mathbf{p}^l &= \boldsymbol{\xi}^l + \frac{\nu_{l-1} - 1}{\nu_l} (\boldsymbol{\xi}^l - \boldsymbol{\xi}^{l-1}), \end{aligned}$$

where l is the iteration index; $\Pi_{\mathcal{X}}(\mathbf{x}) \triangleq \arg \min_{\mathbf{y} \in \mathcal{X}} \|\mathbf{x} - \mathbf{y}\|_2^2$ denotes the projection of \mathbf{x} onto the set \mathcal{X} ; $\nu_{-1} = 0$ and $\nu_l = \frac{1 + \sqrt{1 + 4\nu_{l-1}^2}}{2}$; $\boldsymbol{\xi}^{-1} = \boldsymbol{\xi}^0$ is the initialization; η_l is the step size and is determined by the backtracking line search; see [48] for details.

The computational efficiency of APG hinges on whether the projection $\Pi_{\mathcal{X}}$ can be computed easily. Although the coupling of \mathbf{d} and \mathbf{u}_t 's in the constraints makes the projection seemingly not too easy to compute, it turns out that $\Pi_{\mathcal{X}}$ can be solved in a semi-closed form fashion. Specifically, given a point $\tilde{\boldsymbol{\xi}} = (\tilde{\mathbf{d}}, \tilde{\mathbf{U}})$, the projection $\Pi_{\mathcal{X}}(\tilde{\boldsymbol{\xi}})$ is to solve

$$\begin{aligned} \min_{\mathbf{d}, \mathbf{U}} \sum_{t=1}^T &\|\mathbf{u}_t - \tilde{\mathbf{u}}_t\|_2^2 + \|\mathbf{d} - \tilde{\mathbf{d}}\|_2^2 \\ \text{s.t. } -\mathbf{d} + \mathbf{a}_t &\leq_c \mathbf{u}_t \leq_c \mathbf{d} - \mathbf{c}_t, \quad t = 1, \dots, T, \\ \mathbf{d} &\geq_c \boldsymbol{\alpha}_c. \end{aligned} \tag{31}$$

Observe that Problem (31) is separable w.r.t. each coordinate $i = 1, \dots, K$ and also w.r.t. the real and imaginary components. Hence, solving Problem (31) amounts to solving $2K$ independent subproblems, and all the subproblems share the same structure as follows

$$\begin{aligned} \min_{d, u_1, \dots, u_T} \sum_{t=1}^T &(u_t - \tilde{u}_t)^2 + (d - \tilde{d})^2 \\ \text{s.t. } -d + a_t &\leq u_t \leq d - c_t, \quad t = 1, \dots, T, \\ d &\geq \alpha. \end{aligned} \tag{32}$$

We outline how Problem (32) is solved. The idea is to first eliminate the variables u_t 's by plugging the solutions of u_t 's given d into (32). The resulting problem for d is to solve a series of one-dimensional quadratic programs over different intervals, which admit closed-form solutions. By comparing all solutions of d over all the intervals, the one that gives the smallest objective value is the projection solution. We show the projection solution in Algorithm 1 and the mathematical details are shown in Appendix C.

Algorithm 1 A fast solution to Problem (32)

- 1: **Input:** $[\tilde{u}_1, \dots, \tilde{u}_T, \tilde{d}]$.
- 2: Set $\mathcal{D}_1 \triangleq \{c_t + \tilde{u}_t \mid c_t + \tilde{u}_t \geq \alpha, \forall t\}$.
- 3: Set $\mathcal{D}_2 \triangleq \{a_t - \tilde{u}_t \mid a_t - \tilde{u}_t \geq \alpha, \forall t\}$.
- 4: Set $\tilde{\mathcal{D}} \triangleq \{\alpha\} \cup \mathcal{D}_1 \cup \mathcal{D}_2 \cup \{+\infty\}$.
- 5: Sort the elements of $\tilde{\mathcal{D}}$ in an ascending order to obtain $\mathcal{D} \triangleq \{\omega_1, \dots, \omega_{\text{card}(\mathcal{D})}\}$.
- 6: **For** $p = 1, \dots, \text{card}(\mathcal{D}) - 1$
- 7: Set $\mathcal{T}_p \triangleq \{t \mid \omega_{p+1} \leq c_t + \tilde{u}_t\}$.
- 8: Set $\mathcal{L}_p \triangleq \{t \mid \omega_{p+1} \leq a_t - \tilde{u}_t\}$.
- 9: Compute $d^p = \max\{\omega_p, \min\{\omega_{p+1}, \hat{d}^p\}\}$, where

$$\hat{d}^p = \frac{\sum_{t \in \mathcal{T}_p} (c_t + \tilde{u}_t) + \sum_{t \in \mathcal{L}_p} (a_t - \tilde{u}_t) + \tilde{d}}{1 + \text{card}(\mathcal{T}_p) + \text{card}(\mathcal{L}_p)}.$$

- 10: Compute

$$f^p = \sum_{t \in \mathcal{T}_p} (d^p - c_t - \tilde{u}_t)^2 + \sum_{t \in \mathcal{L}_p} (-d^p + a_t - \tilde{u}_t)^2 + (d^p - \tilde{d})^2.$$

- 11: **End for**

- 12: Compute $d = d^{\tilde{p}}$, where $\tilde{p} = \arg \min_p f^p$.

- 13: Compute $u_t = \max\{-d + a_t, \min\{\tilde{u}_t, d - c_t\}\}, \forall t$.

- 14: **Output:** $[\mathbf{u}_1, \dots, \mathbf{u}_T, d]$.

4.2 Fixing $\mathbf{d} = \boldsymbol{\alpha}_c$, Alternating Minimization over \mathbf{U} and $\boldsymbol{\varphi}$

We propose a suboptimal, but computationally more efficient, alternative of the above SLP design. Specifically we follow the same AM procedure as in the preceding subsection, but we pre-fix the half inter-symbol spacing vector \mathbf{d} as $\mathbf{d} = \boldsymbol{\alpha}_c$ —the same choice as the ZF scheme (19). The minimization of the TTP over (\mathbf{d}, \mathbf{U}) in (29), with $\mathbf{d} = \boldsymbol{\alpha}_c$, is then decoupled into

$$\begin{aligned} \min_{\mathbf{u}_t} & \|\boldsymbol{\alpha}_c \diamond \mathbf{s}_t + \mathbf{u}_t\|_{\mathbf{R}_{\boldsymbol{\varphi}}}^2 \\ \text{s.t. } & -\boldsymbol{\alpha}_c + \mathbf{a}_t \leq_c \mathbf{u}_t \leq_c \boldsymbol{\alpha}_c - \mathbf{c}_t \end{aligned} \tag{33}$$

for $t = 1, \dots, T$. The problems in (33) are (convex) quadratic programs with simple bound constraints. There are numerous ways to solve them efficiently, such as the active set method [49], ADMM [50], and the APG method [51]. We choose the APG algorithm to solve Problem (33); we omit the details since the APG method has been described in the preceding subsection.

We call the above suboptimal SLP scheme the *semi-ZF SLP* scheme, due to the following reason: If $s_{i,t}$ is an ICP, then we have $a_{i,t} = \alpha_{c,i}$, $c_{i,t} = \alpha_{c,i}$; see (9). Consequently, the corresponding symbol

perturbation $u_{i,t}$ is constrained as $0 \leq_c u_{i,t} \leq_c 0$. Hence, we apply symbol perturbations only to points lying on the boundary of the QAM constellation, or outer constellation points (OCPs). It is worth noting that, in the existing works, one indeed employs SLP for OCPs only [24].

5 SLP Schemes for PPAP Minimization

In this section, we describe how our SLP designs can be modified to handle the peak per-antenna power (PPAP) minimization design. The problem is formulated as follows:

$$\begin{aligned} & \min_{\mathbf{X}, \mathbf{d}, \boldsymbol{\varphi}} \max_{t=1, \dots, T} \|\mathbf{x}_t\|_\infty^2 \\ & \text{s.t. } -\mathbf{d} + \mathbf{a}_t \leq_c \boldsymbol{\varphi}^* \circ (\mathbf{H} \mathbf{x}_t) - \mathbf{d} \diamond \mathbf{s}_t \leq_c \mathbf{d} - \mathbf{c}_t, \quad t = 1, \dots, T, \\ & \mathbf{d} \geq_c \boldsymbol{\alpha}_c, \quad |\boldsymbol{\varphi}| = \mathbf{1}, \end{aligned} \quad (34)$$

where we should note that we minimize the PPAP at all the symbol times, which cannot be done by the existing linear precoding formulations.² Substituting the representation (13) to Problem (34) gives

$$\begin{aligned} & \min_{\mathbf{d}, \boldsymbol{\varphi}, \mathbf{U}, \mathbf{Z}} f_{\text{PPAP}}(\mathbf{d}, \boldsymbol{\varphi}, \mathbf{U}, \mathbf{Z}) \\ & \text{s.t. } -\mathbf{d} + \mathbf{a}_t \leq_c \mathbf{u}_t \leq_c \mathbf{d} - \mathbf{c}_t, \quad t = 1, \dots, T, \\ & \mathbf{d} \geq_c \boldsymbol{\alpha}_c, \quad |\boldsymbol{\varphi}| = \mathbf{1}, \end{aligned} \quad (35)$$

where

$$f_{\text{PPAP}}(\mathbf{d}, \boldsymbol{\varphi}, \mathbf{U}, \mathbf{Z}) \triangleq \max_{t=1, \dots, T} \|\mathbf{H}^\dagger(\boldsymbol{\varphi} \circ (\mathbf{d} \diamond \mathbf{s}_t + \mathbf{u}_t)) + \mathbf{B} \mathbf{z}_t\|_\infty^2.$$

Note that the nullspace components \mathbf{z}_t 's, which are shut down in the TTP minimization (cf. Proposition 1), are part of the design variables.

Our optimization strategy is identical to that for TTP minimization in the preceding section. Specifically, we apply AM between $\boldsymbol{\varphi}$ and $(\mathbf{d}, \mathbf{U}, \mathbf{Z})$. The new challenge is that f_{PPAP} is non-smooth. We circumvent this issue by log-sum-exponential (LSE) approximation

$$\max\{x_1, \dots, x_N\} \approx \delta \log \left(\sum_{i=1}^N e^{x_i/\delta} \right), \quad (36)$$

for a given smoothing parameter $\delta > 0$. It is known that the right-hand side of (36) is smooth, and the approximation in (36) is tight when $\delta \rightarrow 0$. Applying (36) to f_{PPAP} yields

$$f_{\text{PPAP}}(\mathbf{d}, \boldsymbol{\varphi}, \mathbf{U}, \mathbf{Z}) \approx \delta \log \left(\sum_{n=1}^N \sum_{t=1}^T e^{\frac{|\tilde{\mathbf{h}}_n^H(\boldsymbol{\varphi} \circ (\mathbf{d} \diamond \mathbf{s}_t + \mathbf{u}_t)) + \tilde{\mathbf{b}}_n^H \mathbf{z}_t|^2}{\delta}} \right) \triangleq \hat{f}_{\text{PPAP}}(\mathbf{d}, \boldsymbol{\varphi}, \mathbf{U}, \mathbf{Z}),$$

where $\tilde{\mathbf{h}}_n^H$ and $\tilde{\mathbf{b}}_n^H$ denote the n th row of \mathbf{H}^\dagger and \mathbf{B} , respectively. The rest of the operations are same as the AM in Section 4.1: we minimize \hat{f}_{PPAP} over $|\boldsymbol{\varphi}| = \mathbf{1}$ by the PG method, and we minimize \hat{f}_{PPAP} over $(\mathbf{d}, \mathbf{U}, \mathbf{Z})$ by the APG method.

²Linear precoding can handle $\max_{n=1, \dots, N} \mathbb{E}[|x_{n,t}|^2]$, the peak per-antenna average power [4]. It cannot handle peak power w.r.t. symbol times, by nature.

Like the suboptimal semi-ZF scheme in Section 4.2, we can pre-fix $\mathbf{d} = \boldsymbol{\alpha}_c$ to reduce the computational cost. It is worthwhile to note that the resulting minimization of \hat{f}_{PPAP} over $(\mathbf{d}, \mathbf{U}, \mathbf{Z})$ with $\mathbf{d} = \boldsymbol{\alpha}_c$ is, in essence, solving

$$\begin{aligned} \min_{\mathbf{u}_t, \mathbf{z}_t} & \|\mathbf{H}^\dagger(\boldsymbol{\varphi} \circ (\boldsymbol{\alpha}_c \diamond \mathbf{s}_t + \mathbf{u}_t)) + \mathbf{B}\mathbf{z}_t\|_\infty^2 \\ \text{s.t. } & -\boldsymbol{\alpha}_c + \mathbf{a}_t \leq_c \mathbf{u}_t \leq_c \boldsymbol{\alpha}_c - \mathbf{c}_t, \end{aligned} \quad (37)$$

for $t = 1, \dots, T$; or, in words, we are minimizing the PPAP of all the symbol times. Moreover, if we further pre-fix $\boldsymbol{\varphi} = \mathbf{1}$ (no phase optimization) and $\mathbf{U} = \mathbf{0}$ (no symbol perturbations), then our design reduces to

$$\min_{\mathbf{z}_t} \|\mathbf{H}^\dagger(\boldsymbol{\alpha}_c \diamond \mathbf{s}_t) + \mathbf{B}\mathbf{z}_t\|_\infty^2 \quad (38)$$

for $t = 1, \dots, T$, which is a nullspace-assisted ZF scheme (more precisely, the design reduces to the LSE approximation of (38)). Our numerical results will show that even the nullspace-assisted ZF scheme provides significant PPAP reduction, compared to the state-of-the-art schemes such as the basic ZF scheme and the linear precoding design under peak per-antenna average power minimization [4].

6 When SLP Meets Vector Perturbation

The SLP designs in the previous sections can also be extended to cover vector perturbation (VP) precoding. To proceed, we first introduce a modulo operation in the decision process at the user side. Specifically, we modify the symbol detection process in (6) by

$$\hat{s}_{i,t} = \text{dec}\left(\mathcal{M}\left(\frac{\Re(\varphi_i^* y_{i,t})}{d_i^R}\right)\right) + \text{j} \cdot \text{dec}\left(\mathcal{M}\left(\frac{\Im(\varphi_i^* y_{i,t})}{d_i^I}\right)\right), \quad (39)$$

where

$$\mathcal{M}(y) = y - \left\lfloor \frac{y + 2L}{4L} \right\rfloor 4L$$

is the modulo operation, with the modulo constant given by $4L$; $\lfloor x \rfloor$ denotes the maximum integer that is less than or equal to x . Such modulo-type detection was introduced in Tomlinson-Harashima precoding [9] and VP precoding [10,11]. Here, we see the detection function (39) as an extension of the previous considered detection function (6), hoping that it can provide additional elbow room for better performance.

Let us investigate SLP under the modulo detection (39). By following the SEP analysis in Section 2, it can be shown that the SEP constraint, $\text{SEP}_{i,t} \leq \varepsilon_i$, is satisfied if

$$-d_i + \alpha_{c,i} \leq_c \varphi_i^* \mathbf{h}_i^H \mathbf{x}_t - d_i \diamond (s_{i,t} + 4L\gamma_{i,t}) \leq_c d_i - \alpha_{c,i}, \quad (40)$$

for some complex integer $\gamma_{i,t}$, i.e., $\gamma_{i,t} \in \mathbb{Z}_C \triangleq \{a + \text{j}b \mid a, b \in \mathbb{Z}\}$, where $\alpha_{c,i} = \alpha_i + \text{j}\alpha_i$ and α_i is defined in (10). Define

$$\boldsymbol{\mu}_t = \boldsymbol{\varphi}^* \circ (\mathbf{H}\mathbf{x}_t) - \mathbf{d} \diamond (s_t + 4L\boldsymbol{\gamma}_t), \quad (41)$$

where $\boldsymbol{\gamma}_t = [\gamma_{1,t}, \dots, \gamma_{K,t}]^T$, such that (40) can be rewritten as

$$-\mathbf{d} + \boldsymbol{\alpha}_c \leq_c \boldsymbol{\mu}_t \leq_c \mathbf{d} - \boldsymbol{\alpha}_c, \quad \forall t.$$

By substituting the representation of \mathbf{x}_t in (13) into (41), the symbol perturbation takes the form

$$\mathbf{u}_t = 4L\mathbf{d} \diamond \boldsymbol{\gamma}_t + \boldsymbol{\mu}_t.$$

We see that the symbol perturbation \mathbf{u}_t consists of two terms. The first term $4L\mathbf{d} \diamond \boldsymbol{\gamma}_t$, or simply $\boldsymbol{\gamma}_t$, is referred to as the vector perturbation; the second term $\boldsymbol{\mu}_t$ plays a similar role as the symbol perturbation \mathbf{u}_t in the previous sections (recall $-\mathbf{d} + \boldsymbol{\alpha}_t \leq_c \mathbf{u}_t \leq_c \mathbf{d} - \boldsymbol{\alpha}_t$ in the previous SLP designs). As a result, the above derivation leads to the transmitted signal \mathbf{x}_t taking the form

$$\mathbf{x}_t = \mathbf{H}^\dagger(\boldsymbol{\varphi} \circ (\mathbf{d} \diamond (\mathbf{s}_t + 4L\boldsymbol{\gamma}_t) + \boldsymbol{\mu}_t)) + \mathbf{B}\mathbf{z}_t. \quad (42)$$

The expression (42) suggests that *SLP under the modulo detection* (39) *takes a form that is the VP extension of the symbol-perturbed, nullspace-assisted, ZF scheme*. In particular, if we choose $\mathbf{d} = \boldsymbol{\alpha}_c$, $\boldsymbol{\varphi} = \mathbf{1}$, $\boldsymbol{\Xi} = \mathbf{0}$ and $\mathbf{Z} = \mathbf{0}$ in (39)-(42), where $\boldsymbol{\Xi} = [\boldsymbol{\mu}_1, \dots, \boldsymbol{\mu}_T]$ and $\mathbf{Z} = [\mathbf{z}_1, \dots, \mathbf{z}_T]$, then the VP precoding scheme

$$\mathbf{x}_t = \mathbf{H}^\dagger(\boldsymbol{\alpha}_c \diamond (\mathbf{s}_t + 4L\boldsymbol{\gamma}_t)), \quad t = 1, \dots, T,$$

is recovered [10].

Next, we specify SLP designs under (39)-(42). The VP-extended SLP designs for TTP minimization and PPAP minimization are, respectively, given by

$$\begin{aligned} & \min_{\mathbf{d}, \boldsymbol{\varphi}, \boldsymbol{\Xi}, \boldsymbol{\Gamma}} \frac{1}{T} \sum_{t=1}^T \|\boldsymbol{\varphi} \circ (\mathbf{d} \diamond (\mathbf{s}_t + 4L\boldsymbol{\gamma}_t) + \boldsymbol{\mu}_t)\|_{\mathbf{R}}^2 \\ & \text{s.t. } -\mathbf{d} + \boldsymbol{\alpha}_c \leq_c \boldsymbol{\mu}_t \leq_c \mathbf{d} - \boldsymbol{\alpha}_c, \quad t = 1, \dots, T, \\ & \quad \boldsymbol{\gamma}_t \in \mathbb{Z}_C^K, \quad t = 1, \dots, T, \\ & \quad \mathbf{d} \geq_c \boldsymbol{\alpha}_c, \quad |\boldsymbol{\varphi}| = \mathbf{1}, \end{aligned} \quad (43)$$

and

$$\begin{aligned} & \min_{\mathbf{d}, \boldsymbol{\varphi}, \mathbf{U}, \mathbf{Z}, \boldsymbol{\Gamma}} \max_{t=1, \dots, T} \|\mathbf{H}^\dagger(\boldsymbol{\varphi} \circ (\mathbf{d} \diamond (\mathbf{s}_t + 4L\boldsymbol{\gamma}_t) + \boldsymbol{\mu}_t)) + \mathbf{B}\mathbf{z}_t\|_\infty^2 \\ & \text{s.t. } -\mathbf{d} + \boldsymbol{\alpha}_c \leq_c \boldsymbol{\mu}_t \leq_c \mathbf{d} - \boldsymbol{\alpha}_c, \quad t = 1, \dots, T, \\ & \quad \boldsymbol{\gamma}_t \in \mathbb{Z}_C^K, \quad t = 1, \dots, T, \\ & \quad \mathbf{d} \geq_c \boldsymbol{\alpha}_c, \quad |\boldsymbol{\varphi}| = \mathbf{1}, \end{aligned} \quad (44)$$

where $\boldsymbol{\Gamma} = [\boldsymbol{\gamma}_1, \dots, \boldsymbol{\gamma}_T]$. Note that, as a direct extension of Proposition 1, we have $\mathbf{Z} = \mathbf{0}$ for TTP minimization.

We apply AM between $\boldsymbol{\varphi}$, $(\mathbf{d}, \boldsymbol{\Xi})$ (respectively $(\mathbf{d}, \boldsymbol{\Xi}, \mathbf{Z})$), and $\boldsymbol{\Gamma}$ for TTP minimization (respectively PPAP minimization). The procedures for handling the $\boldsymbol{\varphi}$ update, $(\mathbf{d}, \boldsymbol{\Xi})$ update and $(\mathbf{d}, \boldsymbol{\Xi}, \mathbf{Z})$ update are the same as in the preceding development. The $\boldsymbol{\Gamma}$ update is done by sphere decoding [52] in the TTP minimization design, and by p -sphere encoding [53] in the PPAP minimization design. We can also consider the semi-ZF scheme wherein we pre-fix $\mathbf{d} = \boldsymbol{\alpha}_c$, as well as the nullspace-assisted ZF scheme (for PPAP minimization) wherein we pre-fix $\mathbf{d} = \boldsymbol{\alpha}_c$, $\boldsymbol{\varphi} = \mathbf{1}$.

The VP extension is numerically found effective in performance improvement, while the downside lies in its higher computational complexity of calling the sphere decoding (or the p -sphere encoding) algorithms.

7 Simulation Results

In this section, we provide numerical results to show the performance of the developed SLP schemes. We aim to shed light onto how different components, such as symbol perturbations and nullspace components, have their respective impacts on the system performance.

The simulation settings are as follows. In each simulation trial, the channel matrix \mathbf{H} is randomly generated and follows an element-wise i.i.d. complex circular Gaussian distribution with zero mean and unit variance. The symbols $s_{i,t}$'s are uniformly drawn from the QAM constellation. The transmission block length is $T = 200$. The power of noise is set to $\sigma_v^2 = 1$. The users share the same SEP requirement, i.e., $\varepsilon_1 = \dots = \varepsilon_K = \varepsilon$. Unless specified, all the results to be reported are results averaged over 100 Monte Carlo simulation trials.

To provide benchmarking, we consider the ZF scheme (19) and the SINR-constrained optimal linear beamforming (OLB) scheme [1, 4, 6]. The implementation of OLB can be found in the supplemental material of this paper.

For clarity, we summarize all the tested precoding schemes in Table 1. We will refer to “SLP” as the SLP design that optimizes all the variables (e.g., Section 4.1 for TTP minimization), “SLP-VP” as the VP extension of “SLP”, “Null-ZF” as the nullspace-assisted ZF scheme, and “Null-VP” as the nullspace-assisted VP scheme.

The implementation details of the SLP algorithms are as follows. For the LSE approximation, we set the smoothing parameter as $\delta = L^2/25$. The AM algorithm terminates when the relative change of the objective values of successive iterations is smaller than 10^{-3} or when the iteration number exceeds 10. The APG method stops when the difference of solutions between successive iterations is smaller than 10^{-3} , or when the iteration number exceeds 300. The PG method is implemented under the same stopping criterion as that of APG. Both Semi-ZF SLP and Null-ZF are initialized with the ZF solution. SLP uses the Semi-ZF SLP solution as the initialization. Null-VP and SLP-VP are initialized by the solutions of VP and Null-VP, respectively.

The remaining parts of this section is organized as follows: Section 7.1 and Section 7.2 show the simulation results of the SLP schemes for TTP minimization and PPAP minimization, respectively. Their VP extensions are considered in Section 7.3.

7.1 SLP for TTP Minimization

First of all, we show the performance of the SLP schemes in the context of TTP minimization. Fig. 2 shows the TTP performance versus the SEP requirement ε for $(N, K) = (32, 30)$ and for various QAM constellation sizes. It is seen that the SLP schemes, both SLP and Semi-ZF SLP, outperform OLB and ZF. Also, the performance gap decreases as the constellation size increases. This trend is in agreement with the result in Theorem 1. We should pay attention to Semi-ZF SLP. For 16-QAM, Semi-ZF SLP outperforms ZF by 5.3dB, which indicates that the designs of the symbol perturbations for OCPs and phase rotations can play a significant role in TTP reduction. Also, it is interesting to see that Semi-ZF SLP exhibits nearly the same performance as SLP, which suggests that the choice of the half inter-symbol spacings $\mathbf{d} = \boldsymbol{\alpha}_c$ is a good heuristic. Note that compared with SLP, Semi-ZF SLP is simpler in structures and much easier to optimize. Thus, Semi-ZF SLP achieves a good balance between high performance and low computational complexity.

Fig. 3 shows the TTP performance versus the problem size K . We set $N = K + 2$, $\varepsilon = 10^{-3}$ and use 16-QAM constellation. It is seen that the TTPs of the SLP schemes increase with K at slower rates than those of OLB and ZF. Again, we see that Semi-ZF SLP works well.

Table 1: Summary of the tested precoding schemes

Name	Scenario	Parameters to optimize	Fixed parameters	Formulations and methods
ZF	TPP	none	$(\mathbf{d}, \varphi, \mathbf{U}) = (\alpha_c, \mathbf{1}, \mathbf{0})$	(19), closed form
	PPAP	none	$(\mathbf{d}, \varphi, \mathbf{U}, \mathbf{Z}) = (\alpha_c, \mathbf{1}, \mathbf{0}, \mathbf{0})$	
OLB [1, 4]	TPP	$(\mathbf{d}, \varphi, \mathbf{U})$	none	(46) in supplemental material, CVX
	PPAP	$(\mathbf{d}, \varphi, \mathbf{U}, \mathbf{Z})$	none	(47) in supplemental material, CVX
Semi-ZF SLP	TPP	(φ, \mathbf{U})	$\mathbf{d} = \alpha_c$	(17), AM with APG and PG
	PPAP	$(\varphi, \mathbf{U}, \mathbf{Z})$	$\mathbf{d} = \alpha_c$	(35), LSE approximation, AM with APG and PG
Null-ZF	PPAP	\mathbf{Z}	$(\mathbf{d}, \varphi, \mathbf{U}) = (\alpha_c, \mathbf{1}, \mathbf{0})$	(35), LSE approximation, APG
SLP	TPP	$(\mathbf{d}, \varphi, \mathbf{U})$	none	(17), AM with APG and PG
	PPAP	$(\mathbf{d}, \varphi, \mathbf{U}, \mathbf{Z})$	none	(35), LSE approximation, AM with APG and PG
VP [10]	TPP	Γ	$(\mathbf{d}, \varphi, \Xi) = (\alpha_c, \mathbf{1}, \mathbf{0})$	(43), sphere decoding
	PPAP	Γ	$(\mathbf{d}, \varphi, \Xi, \mathbf{Z}) = (\alpha_c, \mathbf{1}, \mathbf{0}, \mathbf{0})$	(44), p -sphere encoding
Null-VP	PPAP	(\mathbf{Z}, Γ)	$(\mathbf{d}, \varphi, \Xi) = (\alpha_c, \mathbf{1}, \mathbf{0})$	(44), AM with APG (LSE approximation) and p -sphere encoding
SLP-VP	TPP	$(\mathbf{d}, \varphi, \Xi, \Gamma)$	none	(43), AM with APG, PG and sphere decoding
	PPAP	$(\mathbf{d}, \varphi, \Xi, \mathbf{Z}, \Gamma)$	none	(44), AM with APG (LSE approximation), PG (LSE approximation) and p -sphere encoding

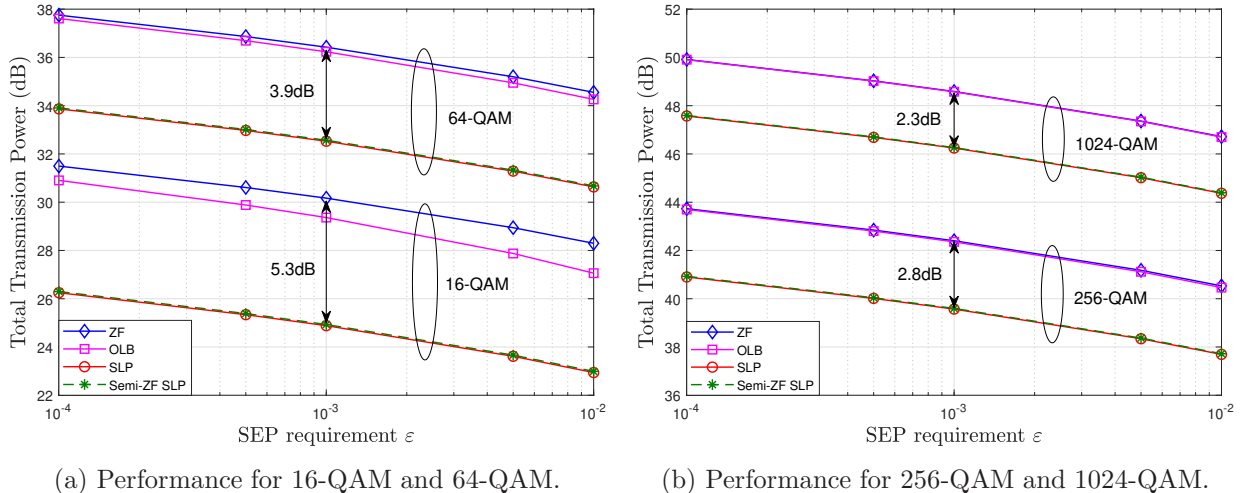


Figure 2: TPP versus the SEP requirements ε . $(N, K) = (32, 30)$.

7.2 SLP for PPAP Minimization

Next, we test the SLP designs for PPAP minimization. We use the complementary cumulative distribution function (CCDF) to measure the PPAP distribution, i.e.,

$$\text{CCDF}(x) = \Pr(\text{PPAP} \geq x).$$

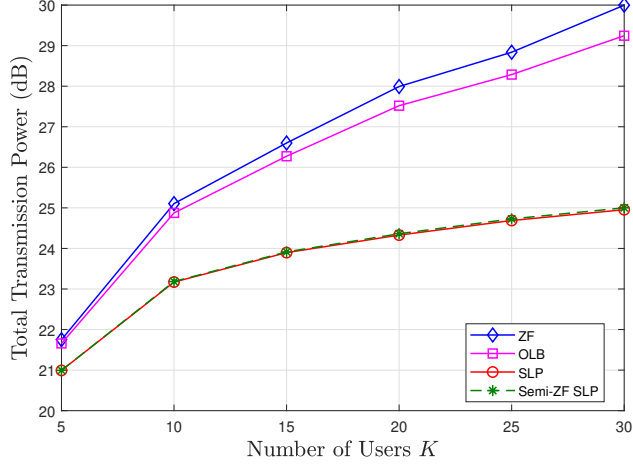


Figure 3: TTP versus the number of users K . $N = K + 2$, $\varepsilon = 10^{-3}$, 16-QAM.

Note that given the same CCDF level, a smaller PPAP threshold x means better performance.

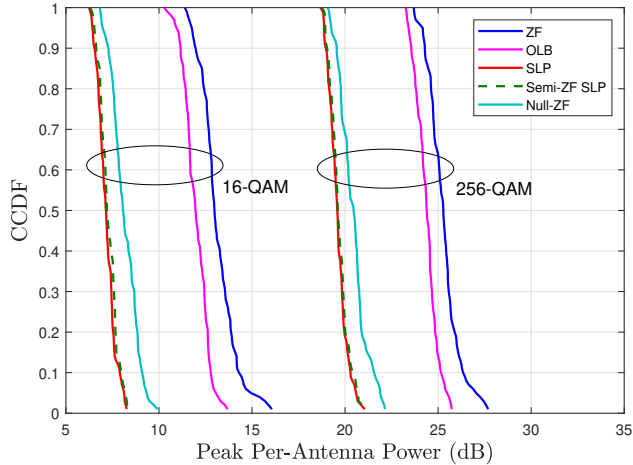


Figure 4: CCDF of PPAP. $(N, K) = (32, 16)$, $\varepsilon = 10^{-3}$.

Fig. 4 presents the CCDF of PPAP for $(N, K) = (32, 16)$ and $\varepsilon = 10^{-3}$. Our observations are as follows. First, all the SLP schemes perform better than the OLB and ZF for 16-QAM and 256-QAM. Different from the TTP minimization case in Fig. 2, in this PPAP minimization case the benefits of SLP over ZF do not vanish as the QAM size increases. Second, Semi-ZF SLP, SLP and Null-ZF provide comparable performance, with Null-ZF performing slightly worse. Comparing Null-ZF with ZF, we see that the incorporation of nullspace components contributes a lot to PPAP reduction. Comparing Null-ZF with Semi-ZF SLP, we see that optimizing the symbol perturbations for OCPs is helpful, though the performance gain is not substantial. Comparing Semi-ZF SLP with SLP, the nearly identical performance of the two again suggests that fixing the half inter-symbol spacings as $\mathbf{d} = \boldsymbol{\alpha}_c$ is a good heuristic. Both Null-ZF and Semi-ZF SLP are computationally light and show promising performance.

Besides the PPAP, we also test the peak-to-average power ratio (PAPR) performance. Specifi-

cally, we evaluate the worst PAPR among all the transmit antennas, defined as $\max_{n=1,\dots,N} \text{PAPR}_n$, where

$$\text{PAPR}_n \triangleq \frac{\max_{t=1,\dots,T} |x_{n,t}|^2}{\sum_{t=1}^T |x_{n,t}|^2 / T}$$

is the PAPR of the n th transmit antenna.

In Fig. 5, we show the CCDF of the worst PAPR for 256-QAM, where $(N, K) = (32, 16)$ and $\varepsilon = 10^{-3}$. We observe similar performance behaviours as the PPAP performance in Fig. 4. Interestingly, although the SLP designs do not minimize the PAPR, the results indicate that minimizing the PPAP is helpful in reducing the PAPR.

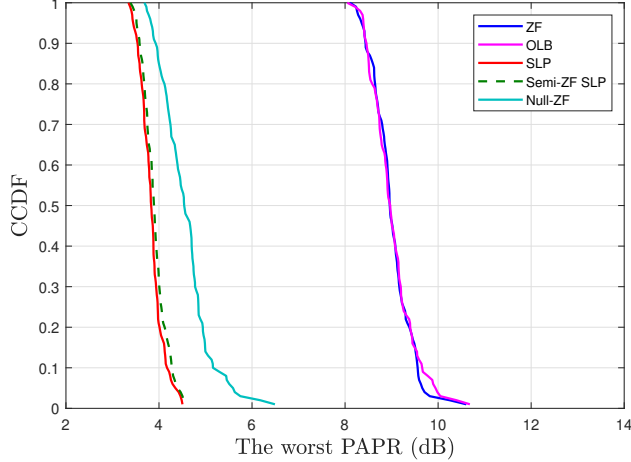


Figure 5: CCDF of the worst PAPR. $(N, K) = (32, 16)$, $\varepsilon = 10^{-3}$, 256-QAM.

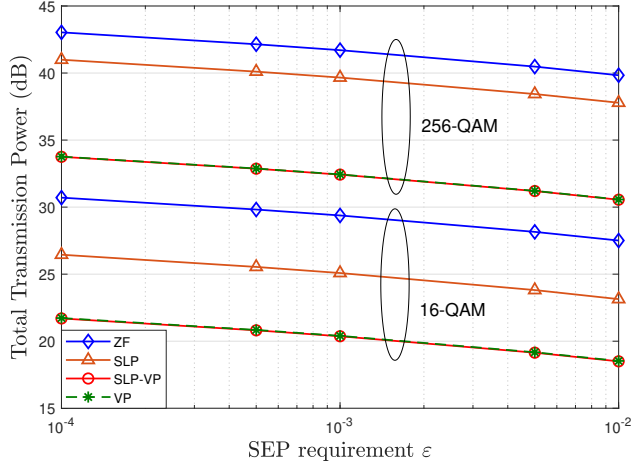


Figure 6: TTP versus the SEP requirements ε for TTP minimization $(N, K) = (16, 15)$.

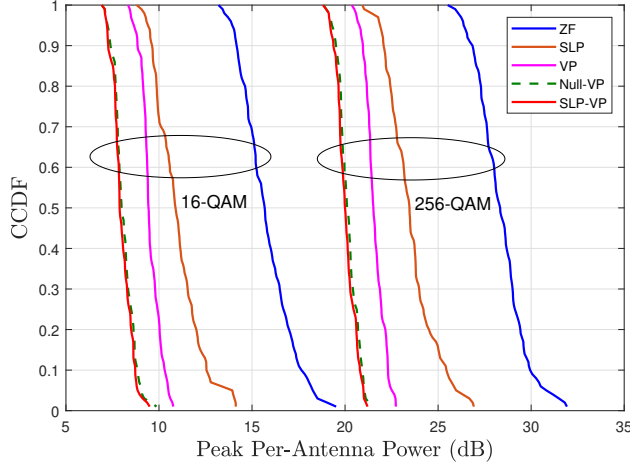


Figure 7: CCDF of the PPAP for PPAP minimization $(N, K) = (16, 8)$, $\varepsilon = 10^{-3}$.

7.3 VP Extension of the SLP Schemes

Finally, we show the performance of the VP extensions of the SLP schemes. We first consider the TTP minimization scenario. The results are shown in Fig. 6, where we evaluate the TTP versus the SEP requirements ε for $(N, K) = (16, 15)$. It is seen that the VP extensions of both SLP and ZF provide much better performance than their no-VP counterparts. We observe that SLP-VP and VP yield nearly identical performance. A possible explanation is as follows. The effect of modulo operation in the detection may be regarded as periodically and infinitely extending the QAM constellation with period $4L$ [11]. Therefore, there is no concept of OCPs for this extended QAM constellation. On the other hand, the numerical results in Section 7.1 suggest that optimizing the symbol perturbations for OCPs is key to improving the performance of the SLP schemes for TTP minimization.

Next, we consider the PPAP minimization scenario. In Fig. 7, we present the CCDF of the PPAP. We choose $(N, K) = (16, 8)$ and $\varepsilon = 10^{-3}$. Again, it is seen that the VP extensions bring significant performance improvement. Moreover, we observe that Null-VP and SLP-VP achieve comparable performance, which again indicates that optimizing the nullspace components plays an important role in PPAP reduction.

8 Conclusion

Through the lens of ZF and VP precoding, we studied SLP under SEP-constrained formulations and under QAM constellations. The connections between SLP, linear precoding and VP precoding were shown by interpreting SLP as a ZF scheme with symbol perturbations, nullspace perturbations, and integer perturbations for the VP extension. Taking insights from these connections, we developed a collection of SLP designs—from a more general design that gives the best performance in principle, to suboptimal but computationally more efficient designs; and from total transmission power minimization to peak per-antenna power minimization. Simulation results were provided to examine the impacts of different design elements on the SLP performance. A summary with our numerical examination is as follows.

1. Symbol perturbations give rise to marked improvement with TTP reduction for lower QAM orders (this is also noted in the literature), but offer little gain once we consider the VP extension.
2. Nullspace perturbations are useless in TTP reduction (this is known analytically), but are instrumental in PPAP reduction.
3. The semi-ZF scheme, which employs a heuristic choice of the half inter-symbol spacings for simplifying the optimization, offers nearly identical performance as the more fully developed SLP designs, which optimizes the half inter-symbol spacings. The same phenomena were observed for the VP extension.
4. The VP-extended SLP designs yield significantly improved performance, although one should note that they also demand higher computational costs because of the need to optimize the integer perturbations.

A Proof of Lemma 1

Problem (20) can be equivalently transformed to

$$\begin{aligned} p^* = \min_{\mathbf{x}} & \|\mathbf{x} + \mathbf{b}\|_{\mathbf{A}}^2 \\ \text{s.t. } & \Re(x_i)^2 \leq \Re(c_i)^2, \quad i = 1, \dots, K, \\ & \Im(x_i)^2 \leq \Im(c_i)^2, \quad i = 1, \dots, K. \end{aligned}$$

The Lagrangian associated with the above problem is

$$\begin{aligned} L(\mathbf{x}, \boldsymbol{\nu}^R, \boldsymbol{\nu}^I) = & \|\mathbf{x} + \mathbf{b}\|_{\mathbf{A}}^2 + \sum_{i=1}^K \nu_i^R (\Re(x_i)^2 - \Re(c_i)^2) \\ & + \sum_{i=1}^K \nu_i^I (\Im(x_i)^2 - \Im(c_i)^2), \end{aligned}$$

where $\boldsymbol{\nu}^R \geq \mathbf{0}$ and $\boldsymbol{\nu}^I \geq \mathbf{0}$ are the dual variables. By the Lagrangian duality theory, it holds that $p^* \geq \inf_{\mathbf{x}} L(\mathbf{x}, \boldsymbol{\nu}^R, \boldsymbol{\nu}^I)$ for any $\boldsymbol{\nu}^R \geq \mathbf{0}$ and $\boldsymbol{\nu}^I \geq \mathbf{0}$. By choosing $\boldsymbol{\nu}^R = \boldsymbol{\nu}^I = \beta \mathbf{1}$ with $\beta \geq 0$, we have

$$\begin{aligned} p^* & \geq \inf_{\mathbf{x}} L(\mathbf{x}, \beta \mathbf{1}, \beta \mathbf{1}) \\ & = \inf_{\mathbf{x}} \{ \|\mathbf{x} + \mathbf{b}\|_{\mathbf{A}}^2 + \beta \|\mathbf{x}\|_2^2 - \beta \|\mathbf{c}\|_2^2 \} \\ & = \mathbf{b}^H (\mathbf{A} - \mathbf{A}(\mathbf{A} + \beta \mathbf{I})^{-1} \mathbf{A}) \mathbf{b} - \beta \|\mathbf{c}\|_2^2, \end{aligned}$$

where the last equation is due to the fact that the optimization problem in the second equation has $\mathbf{x} = -(\mathbf{A} + \beta \mathbf{I})^{-1} \mathbf{A} \mathbf{b}$ as its optimal solution. The proof is complete.

B Proof of Lemma 2

Denote the eigendecomposition of \mathbf{R} as $\mathbf{V} \boldsymbol{\Lambda} \mathbf{V}^H$, where $\mathbf{V} \in \mathbb{C}^{K \times K}$ is unitary and $\boldsymbol{\Lambda} \in \mathbb{C}^{K \times K}$ is diagonal whose diagonal elements are the eigenvalues of \mathbf{R} . We have

$$\mathbf{R}_\varphi = \text{Diag}(\varphi)^H \mathbf{V} \boldsymbol{\Lambda} \mathbf{V}^H \text{Diag}(\varphi) = \hat{\mathbf{V}} \boldsymbol{\Lambda} \hat{\mathbf{V}}^H,$$

where $\hat{\mathbf{V}} = \text{Diag}(\boldsymbol{\varphi})^H \mathbf{V}$. It is seen that $\hat{\mathbf{V}}$ is also unitary. This means that the diagonal elements of $\boldsymbol{\Lambda}$ are also the eigenvalues of \mathbf{R}_φ . Therefore, \mathbf{R}_φ and \mathbf{R} share the same eigenvalues.

From the definition of $\tilde{\mathbf{R}}_\varphi$, we have

$$\begin{aligned}\tilde{\mathbf{R}}_\varphi &= \mathbf{R}_\varphi - \mathbf{R}_\varphi(\mathbf{R}_\varphi + \beta\mathbf{I})^{-1}\mathbf{R}_\varphi \\ &= \hat{\mathbf{V}}(\boldsymbol{\Lambda} - \boldsymbol{\Lambda}(\boldsymbol{\Lambda} + \beta\mathbf{I})^{-1}\boldsymbol{\Lambda})\hat{\mathbf{V}}^H.\end{aligned}$$

It follows that the eigenvalues of $\tilde{\mathbf{R}}_\varphi$ are

$$\lambda_i(\tilde{\mathbf{R}}_\varphi) = \lambda_i(\mathbf{R}) - \frac{\lambda_i^2(\mathbf{R})}{\lambda_i(\mathbf{R}) + \beta} = \frac{\lambda_i(\mathbf{R})\beta}{\lambda_i(\mathbf{R}) + \beta}, \quad \forall i.$$

The proof is complete.

C Derivation of Algorithm 1

Observe from Problem (32) that given $d \geq \alpha$, the optimal u_t 's can be explicitly expressed as

$$u_t = \begin{cases} d - c_t, & \text{if } \tilde{u}_t \geq d - c_t, \\ -d + a_t, & \text{if } \tilde{u}_t \leq -d + a_t, \\ \tilde{u}_t, & \text{otherwise,} \end{cases} \quad (45)$$

for $t = 1, \dots, T$. Therefore, by plugging (45) into Problem (32), the variable to optimize is only d , which leads to a simplified problem. However, different intervals of d will result in different forms of the u_t 's, and thus different forms of the summation term $\sum_{t=1}^T (u_t - \tilde{u}_t)^2$ in the objective function. We next show the formulations for d lying in different intervals. Define the set that includes all the possible boundary points of the intervals of d as

$$\tilde{\mathcal{D}} \triangleq \{\alpha\} \cup \mathcal{D}_1 \cup \mathcal{D}_2 \cup \{+\infty\},$$

where $\mathcal{D}_1 \triangleq \{c_t + \tilde{u}_t, \forall t \mid c_t + \tilde{u}_t \geq \alpha\}$ and $\mathcal{D}_2 \triangleq \{a_t - \tilde{u}_t, \forall t \mid a_t - \tilde{u}_t \geq \alpha\}$. Sort all the elements in $\tilde{\mathcal{D}}$ in ascending order, which results in $\mathcal{D} \triangleq \{\omega_1, \dots, \omega_{\text{card}(\mathcal{D})}\}$ with $\omega_1 \leq \dots \leq \omega_{\text{card}(\mathcal{D})}$. Then, the feasible region of d can be divided into $\text{card}(\mathcal{D}) - 1$ intervals, i.e.,

$$\omega_p \leq d \leq \omega_{p+1}, \quad p = 1, \dots, \text{card}(\mathcal{D}) - 1.$$

By (32) and (45), the optimal d restricted on the p th interval is obtained by solving the following quadratic program:

$$\begin{aligned}\min_d \quad & \sum_{t \in \mathcal{T}_p} (d - c_t - \tilde{u}_t)^2 + \sum_{t \in \mathcal{L}_p} (-d + a_t - \tilde{u}_t)^2 + (d - \tilde{d})^2 \\ \text{s.t.} \quad & \omega_p \leq d \leq \omega_{p+1},\end{aligned}$$

where $\mathcal{T}_p \triangleq \{t \mid \omega_{p+1} \leq c_t + \tilde{u}_t\}$ and $\mathcal{L}_p \triangleq \{t \mid \omega_{p+1} \leq a_t - \tilde{u}_t\}$. The above problem has a closed-form solution given by $d^p = \max\{\omega_p, \min\{\omega_{p+1}, \hat{d}^p\}\}$, where

$$\hat{d}^p = \frac{\sum_{t \in \mathcal{T}_p} (c_t + \tilde{u}_t) + \sum_{t \in \mathcal{L}_p} (a_t - \tilde{u}_t) + \tilde{d}}{1 + \text{card}(\mathcal{T}_p) + \text{card}(\mathcal{L}_p)}.$$

The corresponding optimal value for the p th interval is

$$f^p = \sum_{t \in \mathcal{T}_p} (d^p - c_t - \tilde{u}_t)^2 + \sum_{t \in \mathcal{L}_p} (-d^p + a_t - \tilde{u}_t)^2 + (d^p - \tilde{d})^2.$$

After computing the f^p 's for all p , the d^p that leads to the minimum f^p is the optimal solution to Problem (32).

References

- [1] M. Bengtsson and B. Ottersten, “Optimal and suboptimal transmit beamforming,” in *Handbook of Antennas in Wireless Communications*, L. C. Godara, Ed. Boca Raton, FL, USA: CRC Press, Aug. 2001, ch. 18.
- [2] M. Schubert and H. Boche, “Solution of the multiuser downlink beamforming problem with individual SINR constraints,” *IEEE Trans. Veh. Technol.*, vol. 53, no. 1, pp. 18–28, 2004.
- [3] A. Wiesel, Y. C. Eldar, and S. Shamai, “Linear precoding via conic optimization for fixed MIMO receivers,” *IEEE Trans. Signal Process.*, vol. 54, no. 1, pp. 161–176, 2005.
- [4] W. Yu and T. Lan, “Transmitter optimization for the multi-antenna downlink with per-antenna power constraints,” *IEEE Trans. Signal Process.*, vol. 55, no. 6, pp. 2646–2660, June 2007.
- [5] Y.-F. Liu, Y.-H. Dai, and Z.-Q. Luo, “Max-min fairness linear transceiver design for a multi-user MIMO interference channel,” *IEEE Trans. Signal Process.*, vol. 61, no. 9, pp. 2413–2423, 2013.
- [6] E. Björnson, M. Bengtsson, and B. Ottersten, “Optimal multiuser transmit beamforming: A difficult problem with a simple solution structure,” *IEEE Signal Process. Mag.*, vol. 31, no. 4, pp. 142–148, July 2014.
- [7] Q. Shi, M. Razaviyayn, Z.-Q. Luo, and C. He, “An iteratively weighted MMSE approach to distributed sum-utility maximization for a MIMO interfering broadcast channel,” *IEEE Trans. Signal Process.*, vol. 59, no. 9, pp. 4331–4340, Sep. 2011.
- [8] Q. Shi, M. Razaviyayn, M. Hong, and Z.-Q. Luo, “SINR constrained beamforming for a MIMO multi-user downlink system: Algorithms and convergence analysis,” *IEEE Trans. Signal Process.*, vol. 64, no. 11, pp. 2920–2933, 2016.
- [9] C. Windpassinger, R. F. Fischer, T. Vencel, and J. B. Huber, “Precoding in multiantenna and multiuser communications,” *IEEE Trans. Wireless Commun.*, vol. 3, no. 4, pp. 1305–1316, July 2004.
- [10] B. M. Hochwald, C. B. Peel, and A. L. Swindlehurst, “A vector-perturbation technique for near-capacity multiantenna multiuser communication-part II: Perturbation,” *IEEE Trans. Commun.*, vol. 53, no. 3, pp. 537–544, Mar. 2005.
- [11] J. Maurer, J. Jaldén, D. Seethaler, and G. Matz, “Vector perturbation precoding revisited,” *IEEE Trans. Signal Process.*, vol. 59, no. 1, pp. 315–328, Jan. 2011.

- [12] E. J. Baghdady, "Directional signal modulation by means of switched spaced antennas," *IEEE Trans. Commun.*, vol. 38, no. 4, pp. 399–403, Apr. 1990.
- [13] M. P. Daly and J. T. Bernhard, "Directional modulation technique for phased arrays," *IEEE Trans. Antennas Propag.*, vol. 57, no. 9, pp. 2633–2640, Sep. 2009.
- [14] A. Kalantari, M. Soltanalian, S. Maleki, S. Chatzinotas, and B. Ottersten, "Directional modulation via symbol-level precoding: A way to enhance security," *IEEE J. Sel. Topics Signal Process.*, vol. 10, no. 8, pp. 1478–1493, Dec. 2016.
- [15] C. Masouros and E. Alsusa, "Dynamic linear precoding for the exploitation of known interference in MIMO broadcast systems," *IEEE Trans. Wireless Commun.*, vol. 8, no. 3, pp. 1396–1404, Mar. 2009.
- [16] C. Masouros, "Correlation rotation linear precoding for MIMO broadcast communications," *IEEE Trans. Signal Process.*, vol. 59, no. 1, pp. 252–262, Jan. 2011.
- [17] C. Masouros and G. Zheng, "Exploiting known interference as green signal power for downlink beamforming optimization," *IEEE Trans. Signal Process.*, vol. 63, no. 14, pp. 3628–3640, July 2015.
- [18] A. Haqiqatnejad, F. Kayhan, and B. Ottersten, "Constructive interference for generic constellations," *IEEE Signal Process. Lett.*, vol. 25, no. 4, pp. 586–590, Apr. 2018.
- [19] A. Li and C. Masouros, "Interference exploitation precoding made practical: Optimal closed-form solutions for PSK modulations," *IEEE Trans. Wireless Commun.*, vol. 17, no. 11, pp. 7661–7676, Nov. 2018.
- [20] ——, "Exploiting constructive mutual coupling in P2P MIMO by analog-digital phase alignment," *IEEE Trans. Wireless Commun.*, vol. 16, no. 3, pp. 1948–1962, Mar. 2017.
- [21] M. Alodeh, S. Chatzinotas, and B. Ottersten, "Constructive multiuser interference in symbol level precoding for the MISO downlink channel," *IEEE Trans. Signal Process.*, vol. 63, no. 9, pp. 2239–2252, May 2015.
- [22] ——, "Energy-efficient symbol-level precoding in multiuser MISO based on relaxed detection region," *IEEE Trans. Wireless Commun.*, vol. 15, no. 5, pp. 3755–3767, May 2016.
- [23] J. Krivochiza, A. Kalantari, S. Chatzinotas, and B. Ottersten, "Low complexity symbol-level design for linear precoding systems," in *Proc. Symp. Inf. Theory and Signal Process. Benelux*, 2017.
- [24] M. Alodeh, S. Chatzinotas, and B. Ottersten, "Symbol-level multiuser MISO precoding for multi-level adaptive modulation," *IEEE Trans. Wireless Commun.*, vol. 16, no. 8, pp. 5511–5524, Aug. 2017.
- [25] A. Kalantari, C. Tsinos, M. Soltanalian, S. Chatzinotas, W.-K. Ma, and B. Ottersten, "MIMO directional modulation M-QAM precoding for transceivers performance enhancement," in *Proc. IEEE 18th Int. Workshop Signal Process. Advances Wireless Commun.*, 2017.

- [26] A. Haqiqatnejad, F. Kayhan, and B. Ottersten, “Symbol-level precoding design based on distance preserving constructive interference regions,” *IEEE Trans. Signal Process.*, vol. 66, no. 22, pp. 5817–5832, Nov. 2018.
- [27] M. Alodeh and B. Ottersten, “Joint constellation rotation and symbol-level precoding optimization in the downlink of multiuser MISO channels,” *arXiv preprint arXiv:2011.03935*, 2020.
- [28] C. Studer and E. G. Larsson, “PAR-aware large-scale multi-user MIMO-OFDM downlink,” *IEEE J. Sel. Areas Commun.*, vol. 31, no. 2, pp. 303–313, Feb. 2013.
- [29] M. Yao, M. Carrick, M. M. Sohul, V. Marojevic, C. D. Patterson, and J. H. Reed, “Semidefinite relaxation-based PAPR-Aware precoding for massive MIMO-OFDM systems,” *IEEE Trans. Veh. Technol.*, vol. 68, no. 3, pp. 2229–2243, Mar. 2019.
- [30] R. Liu, M. Li, Q. Liu, and A. L. Swindlehurst, “Secure symbol-level precoding in MU-MISO wiretap systems,” *IEEE Trans. Inf. Forensics Security*, vol. 15, pp. 3359–3373, Apr. 2020.
- [31] M. R. Khandaker, C. Masouros, and K.-K. Wong, “Constructive interference based secure precoding: A new dimension in physical layer security,” *IEEE Trans. Inf. Forensics Security*, vol. 13, no. 9, pp. 2256–2268, Sep. 2018.
- [32] M. Shao, Q. Li, and W.-K. Ma, “Minimum symbol-error probability symbol-level precoding with intelligent reflecting surface,” *IEEE Wireless Commun. Lett.*, vol. 9, no. 10, pp. 1601–1605, 2020.
- [33] D. Spano, M. Alodeh, S. Chatzinotas, J. Krause, and B. Ottersten, “Spatial PAPR reduction in symbol-level precoding for the multi-beam satellite downlink,” in *Proc. IEEE 18th Int. Workshop Signal Process. Advances Wireless Commun.*, 2017, pp. 1–5.
- [34] D. Spano, M. Alodeh, S. Chatzinotas, and B. Ottersten, “Symbol-level precoding for the nonlinear multiuser MISO downlink channel,” *IEEE Trans. Signal Process.*, vol. 66, no. 5, pp. 1331–1345, Mar. 2018.
- [35] S. K. Mohammed and E. G. Larsson, “Per-antenna constant envelope precoding for large multi-user MIMO systems,” *IEEE Trans. Commun.*, vol. 61, no. 3, pp. 1059–1071, Mar. 2013.
- [36] J. Pan and W.-K. Ma, “Constant envelope precoding for single-user large-scale MISO channels: Efficient precoding and optimal designs,” *IEEE J. Sel. Topics Signal Process.*, vol. 8, no. 5, pp. 982–995, Oct. 2014.
- [37] H. Jeddah, A. Mezghani, A. L. Swindlehurst, and J. A. Nossek, “Quantized constant envelope precoding with PSK and QAM signaling,” *IEEE Trans. Wireless Commun.*, vol. 17, no. 12, pp. 8022–8034, Dec. 2018.
- [38] S. Jacobsson, G. Durisi, M. Coldrey, T. Goldstein, and C. Studer, “Quantized precoding for massive MU-MIMO,” *IEEE Trans. Commun.*, vol. 65, no. 11, pp. 4670–4684, Nov. 2017.
- [39] F. Sohrabi, Y.-F. Liu, and W. Yu, “One-bit precoding and constellation range design for massive MIMO with QAM signaling,” *IEEE J. Sel. Topics Signal Process.*, vol. 12, no. 3, pp. 557–570, Jan. 2018.

- [40] M. Shao, Q. Li, W.-K. Ma, and A. M.-C. So, “A framework for one-bit and constant-envelope precoding over multiuser massive MISO channels,” *IEEE Trans. Signal Process.*, vol. 67, no. 20, pp. 5309–5324, Oct. 2019.
- [41] M. Shao, W.-K. Ma, Q. Li, and A. L. Swindlehurst, “One-bit sigma-delta MIMO precoding,” *IEEE J. Sel. Topics in Signal Process.*, vol. 13, no. 5, pp. 1046–1061, Sep. 2019.
- [42] A. Li, C. Masouros, B. Vucetic, Y. Li, and A. L. Swindlehurst, “Interference exploitation precoding for multi-level modulations: Closed-form solutions,” *IEEE Trans. Commun.*, vol. 69, no. 1, pp. 291–308, 2021.
- [43] Y. Liu and W.-K. Ma, “Symbol-level precoding is symbol-perturbed ZF when energy efficiency is sought,” in *Proc. IEEE Int. Conf. Acous., Speech, Signal Process.*, 2018, pp. 3869–3873.
- [44] M. Grant, S. Boyd, and Y. Ye, “CVX: Matlab software for disciplined convex programming,” 2008.
- [45] Z.-Q. Luo, W.-K. Ma, A. M.-C. So, Y. Ye, and S. Zhang, “Semidefinite relaxation of quadratic optimization problems,” *IEEE Signal Process. Mag.*, vol. 27, no. 3, pp. 20–34, May 2010.
- [46] N. Boumal, “Nonconvex phase synchronization,” *SIAM J. Optim.*, vol. 26, no. 4, pp. 2355–2377, 2016.
- [47] J. Tranter, N. D. Sidiropoulos, X. Fu, and A. Swami, “Fast unit-modulus least squares with applications in beamforming,” *IEEE Trans. Signal Process.*, vol. 65, no. 11, pp. 2875–2887, 2017.
- [48] A. Beck, *First-Order Methods in Optimization*. Philadelphia, PA, USA: SIAM, 2017, vol. 25.
- [49] P. B. Stark and R. L. Parker, “Bounded-variable least-squares: an algorithm and applications,” *Computational Statistics*, vol. 10, pp. 129–129, 1995.
- [50] S. Boyd, N. Parikh, E. Chu, B. Peleato, J. Eckstein *et al.*, “Distributed optimization and statistical learning via the alternating direction method of multipliers,” *Foundations and Trends® in Machine learning*, vol. 3, no. 1, pp. 1–122, 2011.
- [51] A. Beck and M. Teboulle, “A fast iterative shrinkage-thresholding algorithm for linear inverse problems,” *SIAM J. Imag. Sci.*, vol. 2, no. 1, pp. 183–202, 2009.
- [52] M. O. Damen, H. El Gamal, and G. Caire, “On maximum-likelihood detection and the search for the closest lattice point,” *IEEE Trans. Inf. Theory*, vol. 49, no. 10, pp. 2389–2402, Oct. 2003.
- [53] F. Boccardi and G. Caire, “The p -sphere encoder: Peak-power reduction by lattice precoding for the MIMO Gaussian broadcast channel,” *IEEE Trans. Commun.*, vol. 54, no. 11, pp. 2085–2091, Nov. 2006.
- [54] J. Proakis, *Digital Communications*, ser. Electrical engineering series. McGraw-Hill, 2001.

Supplemental Material of “Symbol-Level Precoding Through the Lens of Zero Forcing and Vector Perturbation”

Yatao Liu[†], Mingjie Shao[†], Wing-Kin Ma[†] and Qiang Li[‡]

[†]Department of Electronic Engineering, The Chinese University of Hong Kong,
Hong Kong SAR of China

[‡]School of Information and Communication Engineering,
University of Electronic Science and Technology of China, Chengdu, China

March 1, 2025

1 Optimal Linear Beamforming

In this section, we briefly review the optimal linear beamforming (OLB) scheme in [1,4] and describe its implementation in our numerical simulations.

Under the linear precoding scheme $\mathbf{x}_t = \sum_{i=1}^K \mathbf{w}_i s_{i,t}$, the OLB scheme designs the beamforming vectors $\mathbf{w}_1, \dots, \mathbf{w}_K$ by minimizing the average total transmission power (TTP) subject to signal-to-interference-plus noise (SINR) constraints; specifically,

$$\begin{aligned} \min_{\mathbf{w}_1, \dots, \mathbf{w}_K} \mathbb{E}[\|\mathbf{x}_t\|_2^2] &= \sum_{i=1}^K \rho \|\mathbf{w}_i\|_2^2 \\ \text{s.t. } \frac{\rho |\mathbf{h}_i^H \mathbf{w}_i|^2}{\sum_{j \neq i} \rho |\mathbf{h}_j^H \mathbf{w}_j|^2 + \sigma_v^2} &\geq \chi_i, \quad i = 1, \dots, K, \end{aligned} \quad (46)$$

where χ_i is the SINR requirement of the i th user, and $\rho = \mathbb{E}[|s_{i,t}|^2]$. As a variation of (46), we can also consider peak per-antenna average power minimization

$$\begin{aligned} \min_{\mathbf{w}_1, \dots, \mathbf{w}_K} \max_{n=1, \dots, N} \mathbb{E}[|x_{n,t}|^2] &= \sum_{i=1}^K \rho |w_{n,i}|^2 \\ \text{s.t. } \frac{\rho |\mathbf{h}_i^H \mathbf{w}_i|^2}{\sum_{j \neq i} \rho |\mathbf{h}_j^H \mathbf{w}_j|^2 + \sigma_v^2} &\geq \chi_i, \quad i = 1, \dots, K. \end{aligned} \quad (47)$$

In the simulation, the SINR requirement χ_i of both Problems (46) and (47) are chosen to satisfy the symbol-error probability (SEP) requirement (7), which can be achieved by the following fact.

Fact 3 Consider the OLB design in (46) or (47). Suppose that the multiuser interferences (MUIs) are approximated as complex circular Gaussian random variables. Then any feasible beamforming solution to (46) or (47) satisfies the SEP requirements in (7) if we choose

$$\chi_i = \frac{\rho}{2} \left[Q^{-1} \left(\frac{1 - \sqrt{1 - \varepsilon_i}}{2} \right) \right]^2.$$

Proof. Plugging the transmitted signals of the linear precoding scheme (5) into the system model (1), we get

$$y_{i,t} = \mathbf{h}_i^H \mathbf{w}_i s_{i,t} + \underbrace{\sum_{j \neq i} \mathbf{h}_i^H \mathbf{w}_j s_{j,t}}_{\eta_{i,t}} + v_{i,t},$$

where $\eta_{i,t}$ is the MUI. By assuming that $\eta_{i,t}$ is a complex circular Gaussian random variable, we have $\eta_{i,t} \sim \mathcal{CN}(0, \sum_{j \neq i} \rho |\mathbf{h}_i^H \mathbf{w}_j|^2)$. Then, we model

$$\eta_{i,t} + v_{i,t} = \left(\sqrt{\sum_{j \neq i} \rho |\mathbf{h}_i^H \mathbf{w}_j|^2 + \sigma_v^2} \right) \xi_{i,t}, \quad \xi_{i,t} \sim \mathcal{CN}(0, 1).$$

By further assuming that $\mathbf{h}_i^H \mathbf{w}_i \neq 0$, we have

$$\frac{y_{i,t}}{\mathbf{h}_i^H \mathbf{w}_i} = s_{i,t} + \sqrt{\frac{\rho}{\text{SINR}_i}} \xi_{i,t},$$

where

$$\text{SINR}_i = \frac{\rho |\mathbf{h}_i^H \mathbf{w}_i|^2}{\sum_{j \neq i} \rho |\mathbf{h}_i^H \mathbf{w}_j|^2 + \sigma_v^2}.$$

By the basic SEP result in digital communications (e.g. [54]), or by the SEP derivation in Section 2, we have

$$\text{SEP}_{i,t}^R \leq 2Q\left(\sqrt{\frac{2\text{SINR}_i}{\rho}}\right), \quad \text{SEP}_{i,t}^I \leq 2Q\left(\sqrt{\frac{2\text{SINR}_i}{\rho}}\right).$$

By the relation (11) and the invertibility of the Q function, the desired result is obtained. \blacksquare

Problems (46) and (47) can be transformed to convex problems [1] and then solved by available convex optimization softwares, such as CVX [44].

2 The PG Algorithm for Optimizing the Phase Rotation φ

We describe the PG method for tackling optimization problems under unit-modulus constraint; see, e.g. [46, 47]. Consider

$$\min_{|\varphi|=1} f(\varphi), \quad (48)$$

where $f(\varphi)$ is a smooth function. The PG method reads

$$\varphi^{l+1} = \Pi_{|\varphi|=1} \left(\varphi^l - \eta_l \nabla f(\varphi^l) \right),$$

where l is the iteration number; η_l is the step size; the projection operator $\Pi_{|\varphi|=1}$ can be done element-wisely by

$$\mathbf{y} = \Pi_{|\varphi|=1}(\varphi) \Leftrightarrow y_i = \begin{cases} \frac{\varphi_i}{|\varphi_i|}, & \text{if } \varphi_i \neq 0 \\ 1, & \text{otherwise} \end{cases}, \quad \forall i. \quad (49)$$

The choice of the step size η_l should be mentioned. In the TTP minimization case (28), where $f(\varphi) = \varphi^H \bar{\mathbf{R}} \varphi$, we choose $\eta_l = \frac{1}{2\lambda_{\max}(\bar{\mathbf{R}})}$; In the peak per-antenna power (PPAP) minimization case, we employ the backtracking line search [48] to find a step size such that

$$f(\varphi^{l+1}) \leq f(\varphi^l) + \langle \nabla f(\varphi^l), \varphi^{l+1} - \varphi^l \rangle + \frac{1}{2\eta_l} \|\varphi^{l+1} - \varphi^l\|_2^2$$

is satisfied.